A deuterium-poor water reservoir in the asteroid 4 Vesta and the inner solar system

Available online at www.sciencedirect.com

ScienceDirect

Geochimica et Cosmochimica Acta 297 (2021) 203–219

Geochimica et Cosmochimica Acta

www.elsevier.com/locate/gca

A deuterium-poor water reservoir in the asteroid 4 Vesta and the inner solar system

A. Stephant [a,b,c,*], M. Wadhwa [a], R. Hervig [a], M. Bose [a], X. Zhao [b], T.J. Barrett [b], M. Anand [b], I.A. Franchi [b]

[a] School of Earth and Space Exploration, Arizona State University, Tempe, AZ 85287, USA
[b] School of Physical Sciences, The Open University, Milton Keynes, MK7 6AA, UK
[c] Istituto di Astrofisica e Planetologia Spaziali – INAF, 00111 Rome, Italy

Received 14 July 2020; accepted in revised form 4 January 2021; available online 12 January 2021

Abstract

Recent investigations of meteorites thought to originate from the asteroid 4 Vesta have suggested an early accretion of water on rocky bodies in the inner Solar System from a carbonaceous chondrite-like source. However, these studies have been based on the hydrogen isotope compositions (δD) of late-crystallizing apatite grains in eucrites that likely do not record the primary magmatic composition. We have determined the δD and H_2O concentrations in some of the earliest-formed silicates (clinopyroxenes) from several eucrites with the goal of constraining the hydrogen isotope composition of their source reservoir on their parent body. The H_2O concentrations in clinopyroxenes from eucrites Juvinas, Stannern and Tirhert range from 5 to 18 μg/g, with a weighted average δD of –263 ± 70‰. Their apatites and whitlockites exhibit a higher weighted average δD of –165 ± 73‰, possibly as a result of H_2 degassing during or after phosphate crystallization. Thermal metamorphism of these eucrites has most probably resulted in the loss of H, and an increase in their original δD values. While the weighted average δD value for the eucrite clinopyroxenes reported here is inferred to reflect an upper limit for the isotopic composition of the silicate mantle reservoir on their parent asteroid 4 Vesta, the average δD value of Stannern clinopyroxenes is considered to be closest to the initial δD of the source mantle (i.e., –373 ± 127‰), which is lighter than that of Earth's depleted upper mantle and most carbonaceous chondrites. We suggest that at least some of the water in 4 Vesta (and possibly other rocky bodies in the inner Solar System) was derived from a relatively deuterium-poor reservoir in the protosolar nebula, which was incorporated into planetesimals formed early in Solar System history.

Keywords: Eucrites; Vesta; Hydrogen; Deuterium; Water; NanoSIMS

1. INTRODUCTION

Characterizing the abundance and distribution of water (with the term "water" or "H_2O" hereafter referring to $H/OH/H_2O$), as well as the D/H ratio of rocky bodies in the inner Solar System is essential for understanding the source and timescale of water delivery to the terrestrial planets. In this context, the eucrite meteorites are important since they are thought to represent portions of the crust of the asteroid 4 Vesta (McSween et al., 2011; Russell et al., 2013), which is an intact original protoplanet (Russell et al., 2013). Since eucrite minerals crystallized from basaltic magmas ~4.56 Ga ago (e.g., Iizuka et al., 2015; Hopkins et al., 2015; Kleine and Wadhwa, 2017, and references therein), their compositions can provide insights into the

* Corresponding author at: Istituto di Astrofisica e Planetologia Spaziali – INAF, 00111 Rome, Italy.
E-mail address: alice.stephant@inaf.it (A. Stephant).

https://doi.org/10.1016/j.gca.2021.01.004
0016-7037/

compositions of their parent melts and the processes that led to the formation of 4 Vesta's crust during the early history of the Solar System.

Eucrites, mostly composed of pigeonite and calcic plagioclase (McSween et al., 2011; Mittlefehldt, 2015), are grouped into basaltic and cumulate types, based on their petrography (Stolper, 1977; Mayne et al., 2009). The basaltic eucrites are thought to have crystallized rapidly as lava flows at the surface of 4 Vesta, only ~3 to ~10 Ma after the formation of CAIs (McSween et al., 2011) and are composed of fine- to medium-sized grains. Cumulate eucrites, medium- to coarse-grained gabbros, are thought to have crystallized at greater depths, in dikes or plutons (McSween et al., 2011), cooling at a slower rate than basaltic eucrites (over a period of ~150 Ma; McSween et al., 2011), although their parent melts are thought to be very similar (Treiman, 1997; Barrat et al., 2000; Mittlefehldt and Lindstrom, 2003; Barrat, 2004). Among the basaltic eucrites, geochemical subdivision has been established between Main Group-Nuevo Laredo and Stannern trends based on their bulk-rock magnesium number (Mg#) or FeO_{total}/MgO weight ratio, as well as their Ti and incompatible trace element abundances (Stolper, 1977; Hsu and Crozaz, 1996; Hutchison, 2004; Barrat et al., 2007). While the Main Group is widely accepted as a fractional crystallization trend (Stolper, 1977; Warren and Jerde, 1987; Mittlefehldt and Lindstrom, 2003), the Stannern trend eucrites have higher abundances of Ti and incompatible elements, that could be explained as resulting from the contamination of Main Group basaltic melts by crustal melts (Barrat et al., 2007). This contamination model supports the idea that Stannern and some Main Group-Nuevo Laredo trend eucrites erupted contemporaneously (Barrat et al., 2007).

Most eucrites experienced thermal metamorphism, which involved reheating for short duration (about 1 Ma) at a temperature >800–1000 °C (Yamaguchi et al., 1997), several million years after their crystallization (e.g., 13–18 Ma for some Main-Group eucrites; Kleine et al., 2005). Sources of this thermal metamorphism could be either impact melting or heating by subsequent flows or intrusions (Nyquist et al., 1986; Takeda and Graham, 1991). Based on their degree of thermal metamorphism as recorded by the chemical composition of their pyroxenes, eucrites are categorized as ranging from petrologic type 1 to type 7 (Takeda and Graham, 1991; Yamaguchi et al., 1996); increasing metamorphism results in characteristic textural and compositional features in the pyroxene, i.e. loss of chemical zonation, presence of augite lamellae exsolution, and apparent clouding of pyroxenes (Takeda and Graham, 1991).

A range of formation models, involving either partial or extensive melting (magma ocean models) of 4 Vesta, has been proposed to explain the compositional diversity among the eucrites (e.g., Stolper, 1977; Ikeda and Takeda, 1985; Yamaguchi et al., 2009; Mandler and Elkins-Tanton, 2013; Ashcroft and Wood, 2015; Mittlefehldt, 2015 and references therein). However, no single model has yet been able to fully explain the petrographic and geochemical diversity among the Howardite-Eucrite-Diogenite (HED) meteorites (Mittlefehldt, 2015).

The asteroid 4 Vesta is thought to be depleted in volatile elements such as Na and K, as well as H, Cl and F, compared to most rocky planetary bodies (e.g., Karner et al., 2004; Sarafian et al., 2017). Given this volatile depletion, the hydrogen in the regolith observed by the Dawn spacecraft has been concluded to have been supplied by exogenous sources such as water-bearing impactors (Russell et al., 2013; Prettyman et al., 2012). In addition, there is evidence of secondary alteration in several eucrites that is suggested to be mediated by aqueous fluids, possibly derived from exogenous or endogenous sources (Treiman et al., 2004; Barrat et al., 2011). Finally, recent analyses of H-bearing apatites in eucrites, as well as clinopyroxenes, show the presence of water, at least locally in the Vestan interior (Sarafian et al., 2014; Barrett et al., 2016; Sarafian et al., 2019). These studies show that the hydrogen isotope composition of eucritic apatites is similar to that of the Earth's upper mantle and carbonaceous chondrites, raising the possibility that water was acquired from a common chondritic reservoir on all of these inner Solar System rocky bodies (Sarafian et al., 2014; Barrett et al., 2016). These studies additionally argued against late volatile delivery to rocky bodies in the inner Solar System by meteoritic or cometary impactors, tens of millions of years after the beginning of the Solar System (e.g., Albarède, 2009; Halliday, 2013; Sharp, 2017; O'Brien et al., 2018; Piani et al., 2020; Day and Moynier, 2014).

The Ca-phosphate mineral apatite has previously been used as a hygrometer for the Moon (McCubbin et al., 2015a) and 4 Vesta (Sarafian et al., 2017; Barrett et al., 2016) and both hydrogen and chlorine isotopic compositions have been measured in eucritic apatites (Sarafian et al., 2014; Barrett et al., 2016; Sarafian et al., 2017; Barrett et al., 2019). However, inferring the H_2O contents of parent magmas using igneous apatite is not simple (Mathez and Webster, 2005; Boyce et al., 2014; McCubbin et al., 2015b). It has been modelled by Boyce et al. (2014) that H-rich lunar apatites (>1000 μg/g H_2O) could be formed from H-poor parent magmas. In fact, McCubbin et al. (2015b) demonstrated that the interdependence of apatite-melt partition coefficients for F, Cl, and OH induces a large range in the values for the OH partition coefficient. As shown by these authors, if the Cl or F contents of the apatite and the basaltic parent melt are not well constrained, it can result in large uncertainties on the estimation of the H_2O content in the melt in equilibrium with this phase. Furthermore, even if it is possible to calculate the H_2O content in the melt in equilibrium with the apatite, there are other complications. Because apatites are typically among the last crystallizing phases from a melt of basaltic composition, an adequate correction for the amount of crystallization needs to be made to calculate the H_2O content in the parent melt. More importantly, if degassing of H_2 occurred during the crystallization and evolution of the parent melt, the late-forming apatite is unlikely to be a robust indicator of the original H_2O content or D/H ratio of this parent melt (both of which would be significantly affected by dehydrogenation processes). Indeed, H_2 degassing signatures in apatites have been observed in lunar basalts: apatite δD values are often much higher than those

of other early-formed phases (Stephant et al., 2020) or those of their estimated parent melts (Tartèse et al., 2013).

Several studies have shown that nominally anhydrous mineral (NAMs), and in particular clinopyroxenes, can serve as a proxy for quantifying the H_2O content of a basaltic parent melt (Hauri et al., 2006; Wade et al., 2008; O'Leary et al., 2010; Warren and Hauri, 2014). This is because this mineral is one of the first to crystallize from a melt of eucritic basaltic composition and its H_2O partition coefficient for such a melt composition is well constrained (Aubaud et al., 2004; Wade et al., 2008; O'Leary et al., 2010; Warren and Hauri, 2014). However, these partition coefficients were determined at the high pressures of an Earth-like mantle environment (few GPa) and may not be appropriate for asteroidal settings. Moreover, the partition coefficient of hydrogen between melt and pyroxene is dependent on several factors including pressure, oxygen fugacity, and pyroxene Al_2O_3 content (Hauri et al., 2006; Skogby, 2006; Demouchy and Bolfan-Casanova, 2016). Sarafian et al. (2019) determined a partition coefficient between pyroxene and melt of $D = 0.1$ at low pressure (0.1 MPa) and low water content (200 μg/g), which is currently the most appropriate partition coefficient for Vestan conditions. Using this new partition coefficient, they estimate water content in the range of 10–70 μg/g H_2O for bulk 4 Vesta. Here we report the hydrogen isotope compositions and H_2O concentrations in clinopyroxenes and phosphates in three eucritic meteorites measured in situ using secondary ion mass spectrometry (SIMS). We use these data to estimate the hydrogen isotopic composition and the water budget of the asteroid 4 Vesta.

2. MATERIALS AND METHODS

2.1. Standards

Several terrestrial standards were used for the pyroxene and the phosphate analysis sessions. The first set of standards for pyroxene analyses includes San Carlos olivine for background monitoring ($H_2O < 2$ μg/g), KBH-1 orthopyroxene (Koga et al., 2003) for determining instrumental mass fractionation, as well as NMNH 116610–18, NMNH 116610-15, and NMNH 116610-21 clinopyroxenes (Kumamoto et al., 2017) for H_2O calibration. These standards were mounted in 10 mm diameter aluminum boats filled with indium following the protocol established in previous studies (Aubaud et al., 2007; Mosenfelder et al., 2011). As was done previously in several studies of hydrogen in NAMs (Koga et al., 2003; Aubaud et al., 2007; Mosenfelder et al., 2011; Hauri et al., 2002; Tenner et al., 2009), these standards were baked overnight at 115 °C before being pressed into the indium mount. The second set of standards for phosphate analyses includes Dry PMR-53 (which is PMR-53 clinopyroxene that has been dehydrated via heating at 1000 °C for 3 hours, then between 150 °C and 900 °C for 2.5 hours; Bell et al., 1995) for background monitoring, Durango apatite (McCubbin et al., 2010), Macusani rhyolitic glass (Pichavant et al., 1987), DR-15-2-5 and DR20-1-1 (Clog et al., 2013) for determining instrumental mass fractionation and H_2O calibration. These standards were mounted in indium, in the same manner as the first set. Both sets of mounted standards were baked in an oven at 50 °C overnight for ~17 h before being gold-coated and introduced into the NanoSIMS. The H_2O concentrations and δD values of the terrestrial standards are presented in supplementary Table S1.

2.2. Samples

Polished thin sections of three eucrites, Juvinas, Stannern, and Tirhert were studied here (Fig. 1). These eucrites are all observed falls, and the sections were prepared from interior fragments of these meteorites. This aspect is important for minimizing terrestrial exposure (compared to meteorite finds) and contamination of the analyses of H_2O concentrations and D/H ratios conducted here (Stephant et al., 2018). These eucrites represent a variety of crustal materials from the asteroid 4 Vesta. Juvinas and Stannern are noncumulate, basaltic eucrites that are monomict breccias. Geochemically, Juvinas is main group-Nuevo Laredo trend eucrite, whereas Stannern defines the so-called Stannern trend. Unlike the other two, Tirhert is a cumulate, unbrecciated eucrite, and so likely crystallized and cooled more slowly than the other two basaltic eucrites. These three eucrites also belong to different petrologic types representing different degrees of metamorphic equilibration (Takeda and Graham, 1991; Ruzicka et al., 2015): 4 for Stannern, 5 for Juvinas, and 6 for Tirhert. All eucrites higher than type 4 are considered to be equilibrated and are characterized by microscopic or macroscopic pyroxene exsolution features (Takeda and Graham, 1991; Pun and Papike, 1996). Stannern pyroxenes still show remnants of some Mg-Fe zonation that is absent in more metamorphosed eucrites (Takeda and Graham, 1991). Based on the studies of pyroxenes in eucrites (Righter and Garber, 2011; and references therein), Stannern appears to have recorded a complex crystallization, metamorphic (thermal and shock), and brecciation history, which has been summarized by Metzler et al (1995) as follows: (1) crystallization of the primary magma, (2) slow sub-solidus cooling or reheating, (3) impact brecciation, and (4) thermal metamorphism. As such, Stannern has been chemically re-equilibrated to some degree (Metzler et al., 1995), but does not show signs of significant recrystallization and is categorized as type 4. Juvinas pyroxenes do not have any remnant chemical zoning, and contain fine exsolution of augites, as well as homogenous pigeonites clouded with chromite (Takeda and Graham, 1991). As such, the degree of thermal metamorphism evident in Juvinas is higher than in Stannern, such that Juvinas is categorized as type 5. Finally, Tirhert is composed of highly equilibrated plagioclase and pyroxene (that contains exsolution lamellae of augite), and is categorized as type 6 (Ruzicka et al., 2015). The cooling rate associated with type 6 thermal metamorphism is relatively slow and comparable to that of cumulate eucrites, with some of the pigeonite inverted into orthopyroxene (Takeda and Graham, 1991). In fact, cumulate eucrites are considered an unbrecciated sub-set of the petrologic type 6 (Takeda and Graham, 1991).

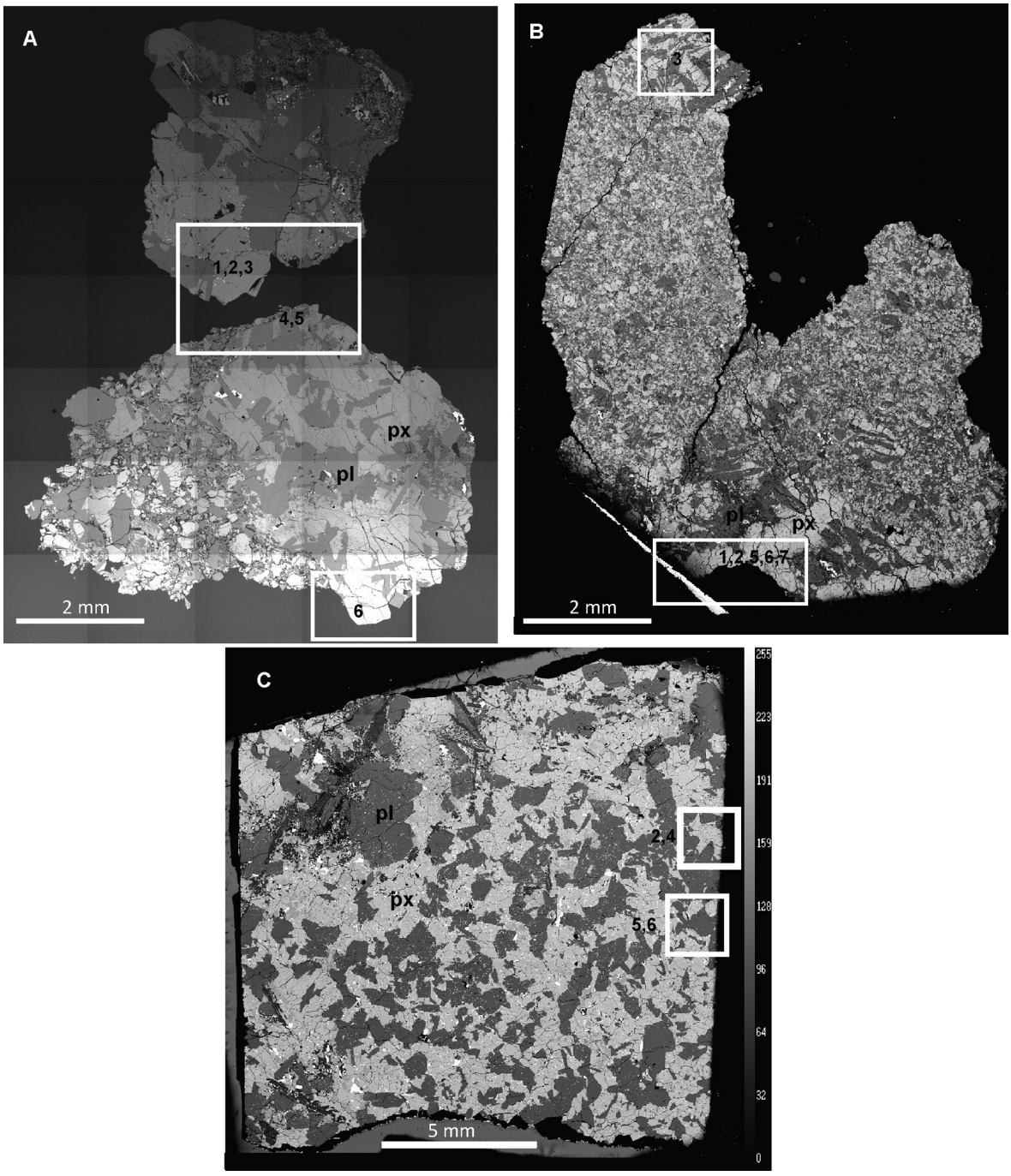

Fig. 1. Backscattered electron images of Juvinas (top left), Stannern (top right), Tirhert (bottom) thin sections. The scale bar is noted at the bottom left of each image.

2.3. Electron microprobe analyses

Backscattered electron (BSE) images and chemical characterization of mineral phases in polished thin sections of Juvinas, Stannern, and Tirhert were obtained on the Cameca SX-100 electron microprobe (Fig. 1). Electron microprobe analyses were made of clinopyroxenes in each of the three eucrites at the Open University after NanoSIMS measurements (adjacent to the NanoSIMS analysis spots). Phosphates were located in Juvinas and Tirhert (supplementary Fig. S1) and were measured at the University of Arizona.

Quantitative mineral analyses were performed in wavelength dispersive mode, with an accelerating potential of 15 kV. A focused beam of 20 nA with a 1 μm spot size was used to analyse the clinopyroxenes, while a beam current of 10 nA with a 10 μm spot size was used for phosphates; ZAF correction was applied to all measurements.

Typical detection limits were 0.02–0.05% for major element oxide abundances. The measured chemical compositions of clinopyroxenes are presented in supplementary Table S2, and those of apatites and whitlockites are presented in supplementary Table S3.

2.4. Secondary ion mass spectrometer analyses

2.4.1. Clinopyroxenes

Secondary ion mass spectrometry measurements of D/H and H/O ratios, calibrated as H_2O concentrations, in clinopyroxenes in Juvinas, Stannern, and Tirhert were performed on the Cameca NanoSIMS 50L at Open University. The H^-, D^-, $^{13}C^-$ and $^{16}O^-$ secondary ions were measured using a Cs^+ primary beam of ~1.4 nA rastered over a $10 \times 10\ \mu m^2$ surface area. The electron gun was tuned to an electron current of approximately 5000 nA. Carbon 13 ions were used to monitor any potential terrestrial contamination on the sample. Examples of NanoSIMS spots on the Juvinas, Stannern, and Tirhert sections analysed here are shown in supplementary Fig. S2. Each analysis surface area was divided into 64×64 pixels, with a counting time of 0.132 ms per pixel. Blanking was performed, and only the $5 \times 5\ \mu m^2$ (25%) interior of the surface area was analysed, with each measurement consisting of 200 cycles. Prior to the analysis, the surface was pre-sputtered for ~10 minutes using the same primary beam current. Vacuum in the analytical chamber was typically $3–3.5 \times 10^{-10}$ Torr.

The H_2O contents in clinopyroxene were determined using a $H^-/^{18}O^-$ versus H_2O calibration (supplementary Fig. S3) based on three terrestrial clinopyroxenes (i.e., 116610-18, 116610-15, and 116610-21; Kumamoto et al., 2017) and the nominally anhydrous San Carlos olivine. The slope of the calibration line determined with the R studio program is $(1.69 \pm 0.07) \times 10^{-7}$. The background for H_2O concentrations in eucrite clinopyroxenes was corrected using the $H^-/^{18}O^-$ ratio measured in the San Carlos olivine, corresponding to a water content of $3 \pm 1\ \mu g/g$ (2SD, $n = 33$). This value was subtracted from each of the H_2O concentration values estimated in the eucrite clinopyroxenes.

The instrumental mass fractionation (IMF) factor was calculated based on analyses of KBH-1, for which D/H ratio was measured by Bell and Ihinger (2000) and Koga et al. (2003). The IMF factor was calculated to be 1.12 ± 0.05 (2SD, $n = 8$). The measured D/H ratios are expressed in terms of δD values, defined as follows in Eq. (1):

$$\delta D = \left[\left(D/H_{sample}\right)/\left(D/H_{VSMOW}\right) - 1\right] \times 1000 \quad (1)$$

where $D/H_{VSMOW} = 155.76 \times 10^{-6}$ (Hagemann et al., 1970). The raw measured D/H ratios were corrected for IMF and the background. Finally, corrections were also applied for the effects of cosmic-ray spallation reactions.

We estimated the production of deuterium by spallation reactions using the D production rate of 2.1×10^{12} mol $D \cdot g^{-1}rock \cdot Ma^{-1}$ (Füri et al., 2017), and the known exposure ages of the eucrites analysed here (Strashnov et al., 2013). This production rate has been estimated based on H_2O-poor olivine and is most appropriate for silicate phases (Füri et al., 2017). The cosmic ray exposure (CRE) ages of Juvinas and Stannern are 11.9 ± 0.5 Ma and 38.9 ± 2.8 Ma (Strashnov et al., 2013), respectively. The exposure age of Tirhert is unknown, as this sample is a relatively recent fall (felt in 2014 in Morocco; Ruzicka et al., 2015). However, it has been established based on their exposure ages that eucrites come from five discrete impact events on 4 Vesta, the youngest of which is 10.6 ± 0.4 Ma and the oldest is 37.8 ± 0.6 Ma (Strashnov et al., 2013). Using the two extreme CRE ages, the CRE-corrected D/H ratios for Tirhert pyroxenes result in δD values that barely overlap with each other within the errors (cf. supplementary Fig. S4). Even though the exact CRE age for Tirhert is not yet known, it is likely to lie within the range of CRE ages of other eucrites. Based on the five impact event cluster ages, the average eucritic exposure age is 22 ± 11 Ma; this value largely incorporates the potential uncertainty in the actual exposure age for Tirhert. As such, we have used this average eucritic exposure age value to correct the D/H ratios in Tirhert pyroxenes for spallation production of deuterium.

The δD value measured for the San Carlos olivine was used to correct the background on the measurements of eucrite clinopyroxenes. The background corrected D/H ratio is obtained using Eq. (2):

$$\begin{aligned} D/H_{corrected} = {} & D/H_{measured}^{(xcorrected)} \\ & \times \frac{H^-/{}^{16}O^-_{measured}}{H^-/{}^{16}O^-_{measured} - H^-/{}^{16}O^-_{background}} \\ & - D/H_{background} \\ & \times \frac{H^-/{}^{16}O^-_{background}}{H^-/{}^{16}O^-_{measured} - H^-/{}^{16}O^-_{background}} \end{aligned} \quad (2)$$

The data for eucrite clinopyroxenes (including the raw $H^-/^{18}O^-$ ratios and background corrected H_2O concentrations, as well as the raw δD values and those corrected for the IMF, background, and spallation effects) are presented in Table 1. Errors estimated for H_2O concentrations take into account the errors from counting statistics and the background. Errors estimated for δD values take into consideration the errors based on counting statistics, as well as the errors in the IMF and on the background δD value.

2.4.2. Phosphate analyses

Measurements of D/H ratios and H/O ratios, calibrated in H_2O concentrations, in the apatites and whitlockites from Juvinas and Tirhert were performed with the Cameca NanoSIMS 50L at Arizona State University. The H^-, D^- and $^{18}O^-$ secondary ions were measured using a Cs^+ primary beam of 150 pA rastered over a $10 \times 10\ \mu m^2$ and a $5 \times 5\ \mu m^2$ surface area for apatites and whitlockites, respectively. Each analysis surface area was divided into 95×95 or 32×32 pixels, with a counting time of 1 ms per pixel. A 300 μm aperture (D1-2) was used and only the interior (50%) of the surface area was analysed, with each measurement consisting of 100–150 cycles. Prior to the analysis, the surface was pre-sputtered for 10 minutes using a primary beam current of 400 pA. The electron gun was tuned to an electron current of roughly 900 nA. A $H^-/^{18}O^-$ vs.

Table 1
The H_2O contents (μg/g) and δD values (‰) measured in pyroxenes of Juvinas, Stannern, and Tirhert determined using the Cameca NanoSIMS 50L at the OU. The H_2O abundances reported here are corrected for the instrumental background. The δD values reported here are corrected for instrumental mass fractionation and background (IMF + bkg. corr.) and are additionally corrected for spallation (spall. corr.). *The spallation correction is done using the production rate in Füri et al. (2017).

Sample	H^-/O^- raw	Error 2SD	H_2O (μg/g) (bkg. corr.)	Error 2SD (μg/g)	δD (‰) raw	δD (‰) (IMF + bkg. corr.)	δD (‰) (spall. corr.)*	Error 2SD (‰)
Juvinas								
Pyroxene 1a	$2.04e^{-07}$	$4.62e^{-10}$	9.3	1.9	51	−98	−266	167
Pyroxene 1b	$1.35e^{-07}$	$3.65e^{-10}$	5.2	1.0	204	83	−215	215
Pyroxene 2	$1.72e^{-07}$	$4.17e^{-10}$	7.4	1.5	138	0	−210	186
Pyroxene 3a	$3.00e^{-07}$	$7.24e^{-10}$	15.0	3.0	27	−110	−214	175
Pyroxene 3b	$2.15e^{-07}$	$6.29e^{-10}$	10.0	2.0	−13	−169	−326	209
Pyroxene 4	$1.89e^{-07}$	$4.16e^{-10}$	8.4	1.7	136	−1	−186	211
Pyroxene 5	$1.46e^{-07}$	$3.70e^{-10}$	5.9	1.2	173	41	−225	199
Pyroxene 6	$1.68e^{-07}$	$4.21e^{-10}$	7.2	1.4	251	138	−78	206
Stannern								
Pyroxene 1a	$2.10e^{-07}$	$4.45e^{-10}$	9.7	1.9	364	261	−268	210
Pyroxene 1b	$2.97e^{-07}$	$4.62e^{-10}$	14.8	2.9	27	−111	−457	180
Pyroxene 2	$3.45e^{-07}$	$1.08e^{-10}$	17.7	3.5	169	40	−250	243
Pyroxene 3	$1.46e^{-07}$	$1.26e^{-10}$	5.9	1.2	541	523	−350	492
Pyroxene 4	$2.08e^{-07}$	$1.97e^{-10}$	9.6	1.9	136	1	−537	471
Pyroxene 5	$1.28e^{-07}$	$4.06e^{-10}$	4.8	1.0	438	412	−660	307
Pyroxene 6	$1.94e^{-07}$	$5.56e^{-10}$	8.7	1.7	248	130	−456	243
Pyroxene 7	$1.49e^{-07}$	$4.24e^{-10}$	6.1	1.2	714	741	−97	291
Tirhert								
Pyroxene 2a	$1.31e^{-07}$	$3.38e^{-10}$	5.0	1.0	605	638	61	422
Pyroxene 2b	$1.86e^{-07}$	$4.32e^{-10}$	8.3	1.6	239	121	−229	338
Pyroxene 4	$2.19e^{-07}$	$4.91e^{-10}$	10.2	2.0	204	78	−205	258
Pyroxene 5	$2.12e^{-07}$	$4.78e^{-10}$	9.8	1.9	194	67	−229	261
Pyroxene 6	$1.61e^{-07}$	$3.80e^{-10}$	6.8	1.3	233	117	−310	376

H_2O calibration curve was used to determine H_2O concentrations in eucrite apatites and whitlockites (supplementary Fig. S5). Background for H_2O concentrations in eucrite apatites and whitlockites is corrected using the $H^-/^{18}O^-$ ratio measured on Dry PMR-53 $(4.36 \pm 0.30) \times 10^{-2}$ (300 ± 20 μg/g) for the analytical session with Juvinas phosphates and $(7.93 \pm 0.62) \times 10^{-2}$ (550 ± 40 μg/g) for the analytical session with Tirhert phosphates).

For hydrogen isotopic measurements, the IMF factor α based on analyses of Durango apatite and Macusani rhyolitic glass standards (supplementary Table S1) is 1.06 ± 0.09 (2SD, n = 9). The measured D/H ratios are expressed in δD notation as defined in equation [1] defined earlier. The raw measured D/H ratios were corrected for IMF, followed by corrections for the background and the effects of spallation reactions. Spallation corrections were applied for water-rich apatites and whitlockites using the D production rate of 9.2×10^{13} mol $D{\cdot}g^{-1}rock{\cdot}Ma^{-1}$ (Merlivat et al., 1976), which was determined on bulk-rock samples and, therefore, is more appropriate production rate for phosphates in the absence of a known phosphate-specific D production rate. The corrected δD values are lower by less than 3‰ compared to uncorrected values, which is significantly smaller than analytical uncertainties. The δD value measured using the Cameca NanoSIMS 50L for the Dry PMR-53 (–139 ± 48‰; 2SD) was used to correct the background on the measurements of eucrite phosphates and did not change over the course of this study. The background corrected D/H ratio is obtained using Eq. (2) defined earlier. The data for eucrite apatites and whitlockites (including the raw $H^-/^{18}O^-$ ratios and background corrected H_2O concentrations, as well as the raw δD values and those corrected for the IMF, background and spallation effects) are presented in Table 2. Errors estimated for H_2O concentrations take into account the errors from counting statistics and the background. Errors estimated for δD values take into consideration the error based on counting statistics, as well as the errors in the IMF and on the background δD value.

3. RESULTS

3.1. Nominally anhydrous minerals

The δD values of nominally anhydrous minerals, i.e., clinopyroxenes, in each of the three eucrites are plotted against H_2O contents in Fig. 2 (data are given in Table 1). The H_2O contents recorded in clinopyroxenes range from 5.2 ± 1.0 to 15.0 ± 3.0 μg/g for Juvinas, from 4.8 ± 1.0 to 17.7 ± 3.5 μg/g for Stannern, and from 5.0 ± 1.0 to 10.2 ± 2.0 μg/g for Tirhert.

Clinopyroxene δD range from –326 ± 209 to – 78 ± 206‰ for Juvinas, from –660 ± 307 to –97 ± 291‰ for Stannern, and from –310 ± 376 to + 61 ± 422‰ for Tirhert. Weighted average of δD in clinopyroxenes is –218

Table 2
The H_2O contents (μg/g) and δD values (‰) measured in whitlockites and apatites of Juvinas and Tirhert determined using the Cameca NanoSIMS 50L at ASU. The H_2O abundances reported here are corrected for the instrumental background. The δD values reported here are corrected for instrumental mass fractionation and background (IMF + bkg. corr.) and are additionally corrected for spallation (spall. corr.). *The spallation correction is done using the production rate in Merlivat et al. (1976).

Sample	Mineral	H^-/O^- raw	Error 2SD	H_2O (μg/g) (bkg. corr.)	Error 2SD (μg/g)	δD (‰) raw	δD (‰) (IMF + bkg. corr.)	δD (‰) (spall. corr.)*	Error 2SD (‰)
Juvinas	Whitlockite 18d	$1.69e^{-01}$	$9.40e^{-03}$	880	78	33	17	16	107
	Whitlockite 19	$2.26e^{-01}$	$3.01e^{-03}$	1282	90	−145	−204	−205	83
	Whitlockite 20	$2.55e^{-01}$	$2.99e^{-03}$	1486	103	−33	−75	−75	96
	Whitlockite 21c	$1.99e^{-01}$	$1.65e^{-03}$	1097	76	178	184	184	126
	Whitlockite 28	$2.62e^{-01}$	$1.22e^{-02}$	1538	128	−113	−166	−166	87
	Whitlockite 31	$1.95e^{-01}$	$1.25e^{-03}$	1065	73	−208	−285	−285	75
	Apatite 23	$2.80e^{-01}$	$6.40e^{-02}$	1665	397	14	−23	−24	134
	Apatite 24	$4.13e^{-01}$	$1.47e^{-02}$	2601	201	−62	−111	−111	91
	Apatite 25	$8.89e^{-02}$	$1.12e^{-03}$	319	22	−10	7	5	116
	Apatite 26	$1.20e^{-01}$	$2.41e^{-03}$	541	39	37	48	47	109
	Apatite 27a	$1.03e^{-01}$	$1.23e^{-03}$	420	29	83	142	141	132
	Apatite 30	$1.30e^{-01}$	$2.91e^{-03}$	608	44	190	257	256	130
Tirhert	Whitlockite 1A	$3.85e^{-01}$	$3.64e^{-02}$	2154	207	−132	−190	−190	76
	Whitlockite 2A	$3.99e^{-01}$	$1.93e^{-02}$	2248	115	−191	−259	−259	70
	Whitlockite 3A	$2.79e^{-01}$	$1.35e^{-02}$	1408	72	−171	−247	−247	71
	Whitlockite 4A	$2.78e^{-01}$	$9.94e^{-03}$	1396	55	−99	−152	−152	80
	Whitlockite 9	$3.50e^{-01}$	$1.66e^{-02}$	1906	96	−22	−58	−58	89
	Whitlockite 14	$3.52e^{-01}$	$7.88e^{-03}$	1920	54	−171	−239	−239	72
	Whitlockite 12	$3.00e^{-01}$	$8.99e^{-03}$	1551	54	−101	−155	−155	80
	Whitlockite 13	$3.85e^{-01}$	$1.02e^{-02}$	2149	68	−171	−236	−236	72
	Apatite 32	$3.91e^{-01}$	$1.34e^{-02}$	2193	84	−218	−292	−292	66
	Apatite 33	$3.81e^{-01}$	$5.65e^{-03}$	2126	48	−217	−292	−292	66

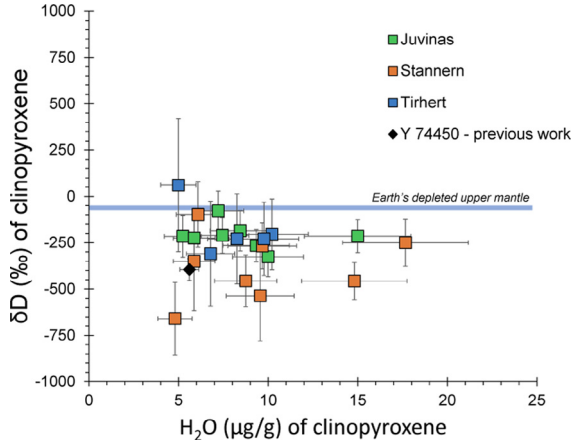

Fig. 2. Plot of δD (‰) versus H_2O (μg/g) in clinopyroxenes of the eucrites analysed here (Juvinas, Stannern, and Tirhert). The value reported for Y-74450 is from Sarafian et al. (2019) and has been corrected for spallation assuming the youngest CRE age for the eucrites (i.e., 7.1 ± 0.6 Ma). Earth's depleted upper mantle δD is given for comparison (60 ± 5‰; Clog et al., 2013).

± 50‰ (2σ, n = 8) for Juvinas, –373 ± 127‰ (2σ, n = 8) for Stannern, and –201 ± 128‰ (2σ, n = 5) for Tirhert. The weighted average of δD for clinopyroxenes in all three eucrites taken together is –263 ± 70‰ (2σ, n = 21). δD averages have been weighted by inverse squares of δD uncertainties.

3.2. Phosphates

The H_2O concentrations and D/H ratios, expressed in δD notation, of apatites and whitlockites in Juvinas and Tirhert are presented in Fig. 3 and Table 2. The H_2O concentrations in apatite and whitlockite of Juvinas range from 319 ± 22 to 2601 ± 201 μg/g and 880 ± 78 to 1538 ± 128 μg/g, respectively. Apatites and whitlockites in Tirhert also exhibit ranges in their H_2O contents, from 2126 ± 48 to 2193 ± 84 μg/g and 1396 ± 55 to 2248 ± 115 μg/g, respectively. The relatively high H_2O content in eucritic whitlockite supports its characterization as this mineral and not as merrillite, which is nominally H-free (Jolliff et al., 2006). Phosphates in Juvinas show a large range of δD values, from –286 ± 75 to + 255 ± 130‰, with a weighted average of – 72 ± 99‰ (average weighted by inverse squares of δD uncertainties). Tirhert phosphates exhibit a narrower range, from –292 ± 66 to –58 ± 89‰, with a weighted average of –223 ± 43‰. The weighted average δD value for all eucrite phosphates measured here is –165 ± 73‰ (2σ, n = 22).

4. DISCUSSION

4.1. Hydrogen isotope and H_2O compositions of clinopyroxenes

Sarafian et al. (2019) reported the water contents for clinopyroxenes in a set of eucrites (Yamato (Y)-74450, Y-75011, Y-793548, Y-82210, as well as Juvinas). The water

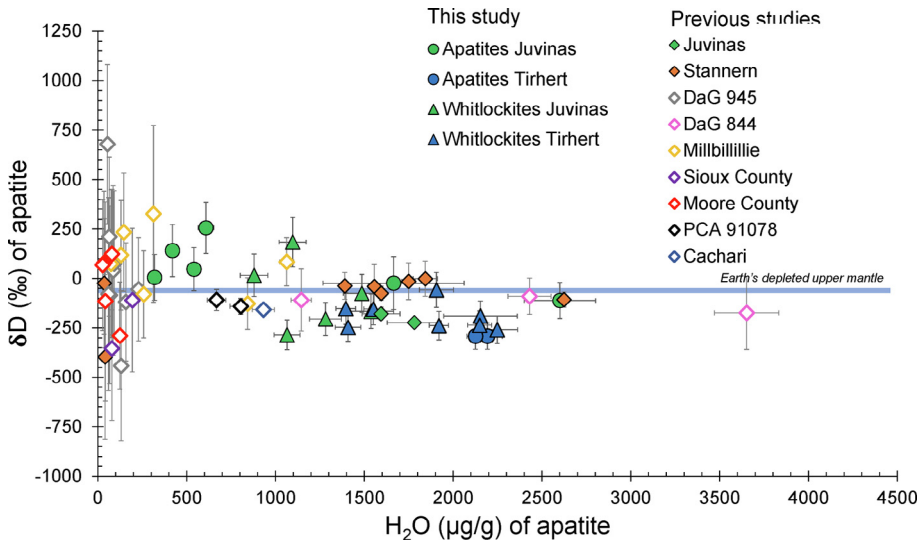

Fig. 3. Plot of δD (‰) vs. H_2O (µg/g) in apatites and whitlockites of Juvinas and Tirhert, compared to literature data. Data for phosphates from Dar al Gani (DaG) 844, DaG 945, Millbillillie, Stannern, Sioux County, and Moore County are from Barrett et al. (2016); data for phosphates from Pecora Escarpment (PCA) 91078, Juvinas, Stannern, and Cachari are from Sarafian et al. (2014). Earth's depleted upper mantle δD is given for comparison (60 ± 5‰; Clog et al., 2013).

content ranges from 1.8 ± 0.2 to 9.9 ± 1.0 µg/g for clinopyroxenes in the Yamato eucrites (n = 8) and from 3.7 ± 0.4 to 4.4 ± 0.4 µg/g in the two Juvinas pyroxenes analysed. The lower content of water in the cores of Juvinas pyroxenes compared to those in the unequilibrated Yamato eucrites is inferred as evidence that thermal equilibration of eucrites occurred in an open system for H (Sarafian et al., 2019). Our analyses of clinopyroxenes in the three equilibrated eucrites, Juvinas, Stannern, and Tirhert yield a slightly broader range of water contents compared to those in the unequilibrated Yamato eucrites, with an average value of 8.8 ± 3.4 µg/g H_2O. Nevertheless, there is some indication that the water content of eucritic clinopyroxenes is related to the degree of metamorphic equilibration of the samples (Fig. 4). While the lowest H_2O values measured in clinopyroxenes in the three samples analysed here are the same within errors, the least thermally metamorphosed Stannern shows the highest average water content (i.e., 9.6 ± 4.5 µg/g H_2O) and the largest range in water abundances, while the more thermally metamorphosed Tirhert shows the lowest average water content (i.e., 8.0 ± 2.2 µg/g H_2O) and the smallest range in water abundances (Fig. 4). Moreover, no correlation is observed between the Mg# (Mg/(Mg + Fe)) of clinopyroxenes and their water content (supplementary Fig. S6), which should be expected if only fractional crystallization played a role in H incorporation in the pyroxenes. Indeed, due to the incompatibility of H, a later-formed pyroxene (with a lower Mg#) should incorporate higher amounts of H compared to an earlier-formed (higher Mg#) pyroxene, resulting in a negative Mg#-H_2O trend. Such a trend is not observed for pyroxenes in the three eucrites studied here (supplementary Fig. S6). As such, it is possible that the water contents (and perhaps also δD values) in the most thermally metamorphosed eucrites such as Tirhert may have been affected to some degree by secondary subsolidus processes.

Only a single value of δD (i.e., –228 ± 49‰) has previously been reported for a eucritic pyroxene (in Yamato 74450; Sarafian et al., 2019). This value is not corrected for spallation as the exposure age of this eucrite is unknown and the authors stated that the correction would be small, on the order of few 10 s of permil. Nevertheless, pyroxene in this eucrite has a water content of 5.6 ± 0.5 µg/g (average of the three measurements reported by Sarafian et al., 2019), which is likely to result in a non-negligible correction. The exposure ages measured so far in eucrites vary from 7.1 ± 0.6 Ma to 38.9 ± 2.8 Ma, and are apparently related to five distinct impact events (Strashnov et al., 2013). Using the lowest value as a minimum, the minimal spallation correction of this pyroxene would be 167‰, giving a corrected δD value of –395 ± 54‰. This minimal spallation-corrected value of the unequilibrated Yamato 74450 is consistent with the weighted average of clinopyroxene δD values measured in Stannern (−373 ± 127‰), the least thermally metamorphosed eucrite in our sample set. Indeed, while the weighted averages of clinopyroxene δD values in each of the three eucrites are indistinguishable from each other within their uncertainties (Fig. 4A), the absolute values of these weighted averages and the δD ranges in clinopyroxenes in each of these eucrites seem to correlate with their degree of metamorphism (Fig. 4; supplementary Fig. S7). Pyroxene in the least thermally altered sample, Stannern, has a lower weighted average δD (−373 ± 127‰) compared to that for the most altered sample, Tirhert (−201 ± 128‰). Student T-test among these samples confirm this significant δD difference (p value <0.05). This is further supported by the similarity of δD in pyroxene for Stannern and for the unequilibrated Yamato 74450 (Sarafian et al., 2019). Therefore, this correlation, although somewhat tenuous, might indicate that some (likely diffusive) loss of H from the clinopyroxene during thermal metamorphism may have resulted in systematically higher δD

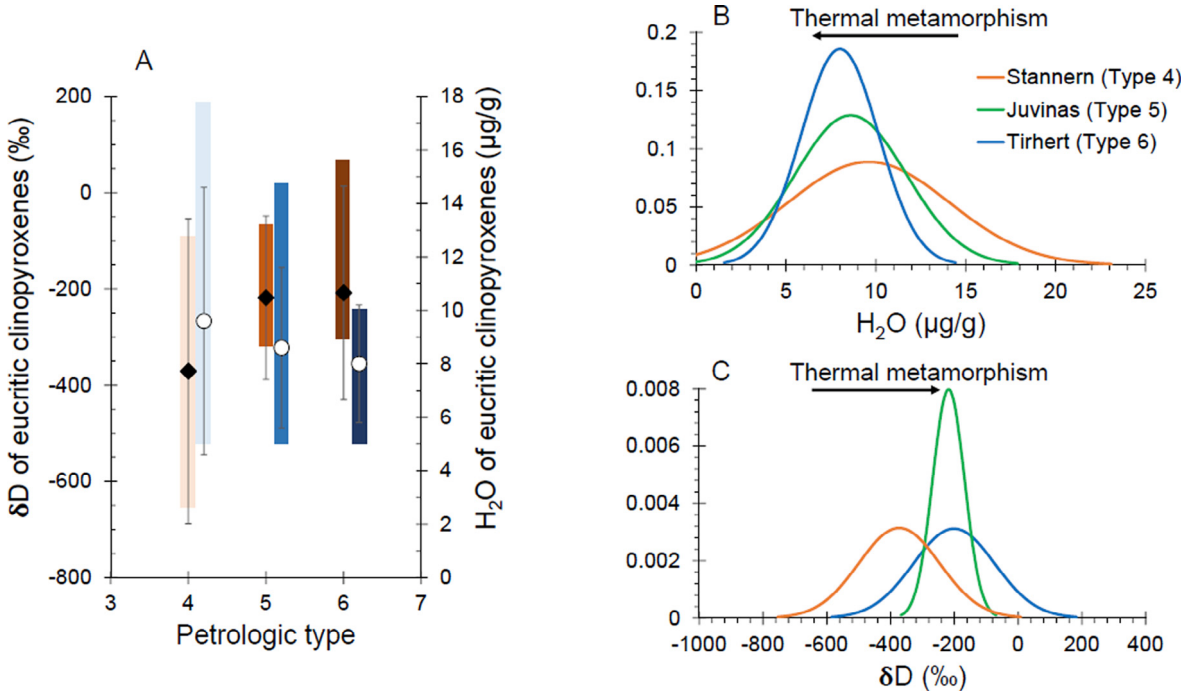

Fig. 4. (A) Ranges of δD (vertical brown bars) and H_2O (vertical blue bars) measured in clinopyroxenes of the three eucrites as a function of their petrologic type indicating thermal metamorphic grade (Stannern = 4; Juvinas = 5; Tirhert = 6). Diamond symbols (with ±2SD errors) represent weighted averages of δD values and circle symbols (with ±2SD errors) represent averages of water concentrations in clinopyroxenes. (B) Gaussian plot of H_2O (µg/g) in clinopyroxenes of the eucrites analysed here (Juvinas, Stannern, and Tirhert). Eucrites with a higher degree of thermal metamorphism exhibit lower average water contents in their clinopyroxenes. (C) Gaussian plot of δD (‰) in clinopyroxenes of the eucrites analysed here (Juvinas, Stannern, and Tirhert). Eucrites with a higher degree of thermal metamorphism exhibit higher average δD values in their clinopyroxenes, which is apparent from higher δD values measured in the sample (see main text for explanation). (For interpretation of the references to color in this figure legend, the reader is referred to the web version of this article.)

and lower H_2O contents (Kyser et al., 1998; Bindeman et al., 2013).

4.2. Hydrogen isotope and H_2O compositions of phosphates

The δD values for Juvinas and Stannern apatites have been previously reported to range from –223 ± 21 to –179 ± 29‰ and from –107 ± 38 to –37 ± 68‰, respectively (Sarafian et al., 2014; Barrett et al., 2016, additionally reported data for Stannern apatites that have significantly larger errors but agree with these values) (Fig. 3). Overall, the eucritic apatite data set from Sarafian et al. (2014), including PCA 91078, Pasamonte, Juvinas, Stannern and Cachari, yields a weighted average δD of –162 ± 127‰. Barrett et al. (2016) have also reported data for apatites from the DaG 945, DaG 844, Millbillillie, Stannern, Sioux County, and Moore County eucrites. The weighted average δD reported by these authors is –34 ± 67‰, consistent with the data of Sarafian et al. (2014) (Fig. 3).

In this study, we analysed phosphates from Juvinas and Tirhert that yield a weighted average δD of –165 ± 73‰, which is indistinguishable from the weighted average of the δD values of eucritic apatites of –151 ± 23‰ obtained from the combined data sets of Sarafian et al. (2014) and Barrett et al. (2016). Based on the similarity of this δD value with that of bulk carbonaceous chondrites (Robert, 2003; Alexander et al., 2012) and the depleted upper mantle of Earth (Clog et al., 2013), these previous studies inferred that water on 4 Vesta and Earth was derived from a carbonaceous chondrite-like reservoir.

However, the weighted average δD value reported here for eucritic clinopyroxenes is lighter than such reservoirs (Fig. 5). Terrestrial contamination is an unlikely explanation for the relatively heavier weighted average δD value for apatites and whitlockites in the Juvinas and Tirhert eucrite falls as their water contents are relatively high (~300 to ~2600 µg/g). Notably, the lowest δD values measured in these eucritic phosphates (i.e, δD = –285 ± 75‰ in Juvinas whitlockite and – 292 ± 66‰ for Tirhert apatite) are close to the weighted average value for eucritic clinopyroxenes (i.e. –263 ± 70‰; Fig. 5). Furthermore, there appears to be a slight negative correlation between δD values and H_2O contents in these eucritic phosphates (in particular for Juvinas and Tirhert; Fig. 3). This trend could be the result of H_2 degassing from the magma during phosphate crystallization (Kyser and O'Neill, 1984). In fact, the Cl isotopic compositions of apatites in eucrites have been argued to result from degassing during a magma ocean crystallization phase of 4 Vesta (Sarafian et al., 2017; Barrett et al., 2019). However, the δD and δCl signatures in eucritic apatites appear to be decoupled, and Cl is thought to have degassed as metal chloride in a H-poor environment. Alternatively, a similar trend could result from subsolidus diffusive loss of hydrogen from the

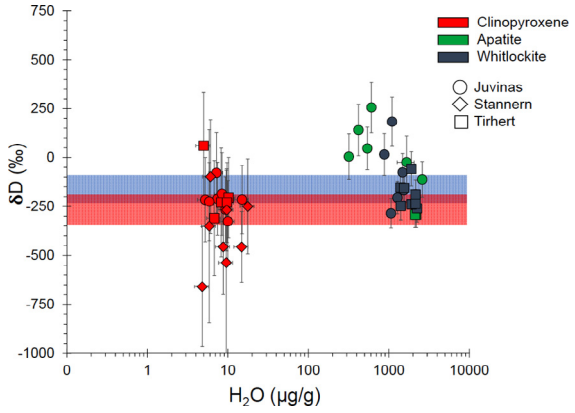

Fig. 5. Plot of δD (‰) versus H_2O (µg/g) in clinopyroxenes (red), apatites (green) and whitlockites (blue) of the eucrites analysed here (Juvinas, Stannern, and Tirhert). The red band is the weighted average of the δD values (–263 ± 70‰) in the clinopyroxenes of these three eucrites. The δD values obtained here for phosphates, i.e., apatites and whitlockites, from Juvinas and Tirhert are consistent with previously reported data for eucritic apatites (Sarafian et al., 2014; Barrett et al., 2016); the weighted average δD value for these phosphates analysed in this study of –165 ± 73‰ is shown as the blue band. (For interpretation of the references to color in this figure legend, the reader is referred to the web version of this article.)

phosphates (see below). As such, the Juvinas and Tirhert phosphates with the highest H_2O contents likely record δD values (i.e., ~–300‰) that represent an upper limit for the mantle source on 4 Vesta.

4.3. Possible processes affecting eucritic clinopyroxenes: Implications for the hydrogen isotopic composition of 4 Vesta

Considering (i) the low water concentrations, (ii) the low δD values, and (iii) the equilibrated nature of clinopyroxenes in the eucrites studied here, it is important to evaluate the reliability of clinopyroxene H_2O-δD systematics to infer the origin and abundance of water on 4 Vesta. Here we assess the different processes that might have altered the initial H_2O-δD signatures in eucritic clinopyroxenes.

One might consider that NAMs are more prone to terrestrial alteration than the relatively water-rich minerals such as phosphates because of their low H_2O content (Stephant et al., 2018). The three eucrites studied here are all falls, so that they had limited exposure to the terrestrial environment. We also ensured that the polished sections were prepared from interior fragments of these meteorites. We followed well-established SIMS protocols to minimise H contamination during analyses (see Sections 2.4.1 and 2.4.2). Moreover, the high spatial resolution of the NanoSIMS technique allows for the avoidance of cracks (that can serve as pathways for contamination) during analyses. We note that the δD weighted average obtained for eucritic pyroxenes, i.e., –263 ± 70‰, is lower than terrestrial water reservoirs (–130 to + 10‰, with the exception of ice sheets; Lécuyer et al., 1998), also suggesting minimal terrestrial alteration in these minerals.

Equilibrium isotopic fractionation of hydrogen can occur in a basaltic system and the effect varies with temperature (Saccocia et al., 2009). However, the fractionation among minerals for a given temperature is limited to ~60‰ (Saccocia et al., 2009). Moreover, Bindeman et al. (2012) demonstrated through modelling of melting processes that no significant hydrogen isotopic fractionation is expected during basaltic melt crystallization. As such, any large variations among phases within a basalt have to be the result of other processes, such as degassing, diffusion, or contamination (Kyser and O'Neill, 1984; Bindeman et al., 2012).

While degassing leads to a decrease in the total H_2O content of the magma, the effects on magmatic δD values can vary depending on the H-bearing species that is being degassed (Kyser and O'Neill, 1984), i.e., loss of H_2O from a parent magma decreases the magmatic δD value while loss of H_2 increases δD. Therefore, if H_2O loss occurs from the magma during crystallization, a positive correlation between δD and H_2O content is expected between earlier-formed and later-formed crystals. However, at the temperature at which basaltic magmas degas (i.e., ~1200 °C), the D/H ratios of the H_2O vapor and basaltic minerals are nearly identical such that no fractionation in D/H ratio is expected (Kyser and O'Neill, 1984; Sarafian et al., 2017). Furthermore, given the relatively low oxygen fugacity within 4 Vesta (i.e. $\Delta IW \sim -2.2$ for Vesta; Righter and Drake, 1996), the dominant H–bearing species degassed from eucrite magmas is expected to be H_2 and not H_2O (Sarafian et al., 2014; Hirschmann et al., 2012). The loss of H_2 from the magma during crystallization would result in an anti-correlation between δD and H_2O content. However, clinopyroxenes in Juvinas, Stannern, and Tirhert do not show any clear evidence (i.e., outside of the analytical uncertainties) for such an anti-correlation within or among these eucrites.

Subsolidus diffusive loss of hydrogen from minerals can also lead to an anti-correlation between δD and H_2O content; this is due to the relatively rapid diffusion of protons compared to deuterons from a solid phase to the surrounding phase(s) (Roskosz et al., 2018). Within each of the eucrites studied here, the clinopyroxenes do not exhibit such trends (Fig. 2). This would suggest that neither degassing nor subsolidus diffusive loss have significantly affected the δD-H_2O systematics in clinopyroxenes within these eucrites (in contrast to the phosphates discussed earlier in Section 4.2 which may record the effects of such processes in their δD-H_2O systematics).

Nevertheless, as discussed previously in Section 4.1, Fig. 4 provides a hint that diffusive equilibration due to thermal metamorphism may have affected the H_2O-δD systematics in clinopyroxenes to a minor degree among various eucrites. Specifically, our results on the three eucrites with different degrees of equilibration suggest that the higher the degree of thermal metamorphism, the higher the weighted average δD of clinopyroxenes and the lower the water content (Fig. 4 and supplementary Fig. S7). As such, it seems plausible that subsolidus thermal metamorphism has induced H^+ diffusion through the pyroxenes, resulting in an increase of the original δD and a decrease

of the H_2O content. It is noteworthy that the bulk sample of Juvinas has heavier rubidium and potassium isotopic compositions compared to the bulk sample of Stannern (supplementary Fig. S7; Pringle and Moynier, 2017; Tian et al., 2019). This is consistent with volatile losses during planetary processes rather than during nebular processes (Pringle and Moynier, 2017), even though the actual process responsible for such loss is unclear (Tian et al., 2019). It is possible that the thermal metamorphism of eucrites might have been responsible for some of these volatile losses. Therefore, among our sample set, Stannern, with the lowest degree of thermal metamorphism, could be viewed as the best proxy for constraining 4 Vesta's water abundance and hydrogen isotopic composition notwithstanding its complex petrological history. Moreover, among the three eucrites studied here, the weighted average δD value for Stannern clinopyroxenes (i.e., –373 ± 127‰; 2SD, n = 8) is closest to the minimally spallation-corrected δD value for clinopyroxenes in the Yamato 74450 unequilibrated eucrite (i.e., –395 ± 54‰; uncorrected δD value = –228 ± 49‰ from Sarafian et al., 2019) which was largely unaffected by thermal metamorphism.

Solar wind hydrogen (with a δD of ~–1000‰; Wiens et al., 2004) can be implanted in mineral grains (up to a depth of a few 100 s of nm) at the surfaces of airless bodies. Indeed, agglutinates in lunar soil are known to have very light δD signatures (e.g. Liu et al., 2012; Stephant and Robert, 2014) that are attributed to solar wind incorporation in the lunar regolith due to space weathering. Implanted solar wind hydrogen could then be incorporated into lunar magmas by assimilation of this regolith, thereby leading to a lowering of the original magmatic δD. Such processes have been suggested to account for low δD values measured in some lunar mare basalts (Treiman et al., 2016; Singer et al., 2017; Barnes et al., 2019). Assimilation of lunar regolith, associated with light δD signatures, in magmas erupting at the lunar surface has also been implicated in the petrogenesis of some highly fractionated rocks such as quartz-monzodiorites (QMDs) and felsites (e.g. Robinson et al., 2016). However, there is no petrographic or geochemical evidence of regolith assimilation in the eucrites studied here. As such, assimilation of solar wind implanted surface materials in the parent melts is likely to be an insignificant factor for these eucrites.

Finally, δD correction from spallation contributions of deuterium can be an important issue, considering the typically low water content in the pyroxenes. However, CRE ages of eucrites are well determined and relatively low, i.e., between 7.1 and 39.7 Ma (Strashnov et al., 2013). Tirhert is an exception, as being a relatively recent fall, its exposure age is still undetermined. However, we can assume that the average CRE age for eucrites of 22 ± 12 (estimated from the average of the exposure ages of the five eucrite clusters; Strashnov et al., 2013) is the best estimate for the exposure age of Tirhert.

In light of the above discussion, we conclude that the weighted average δD of clinopyroxenes of the eucrites Juvinas, Stannern, and Tirhert (i.e., –263 ± 70‰) reflects the upper limit of the composition of the eucrite parent magmas, and that for Stannern clinopyroxenes (i.e., –373 ± 127‰) may be considered to be the closest proxy for the initial δD of the mantle source reservoir of the eucrites on 4 Vesta. As noted previously, this weighted average value for Stannern pyroxenes is similar to the minimally spallation-corrected value for pyroxene in the unequilibrated Yamato 74450 eucrite (i.e. –395 ± 54‰; spallation uncorrected δD value = –228 ± 49‰ from Sarafian et al., 2019), which is largely unaffected by thermal metamorphism. This is lower than the weighted average δD of the phosphates in Juvinas and Tirhert (i.e., –165 ± 73‰), but still consistent within errors, with the δD value measured in the phosphate with the highest H_2O content (i.e., –292 ± 66‰ in a Tirhert apatite; Table 1). Since the D/H fractionation between these magmas and their source in the Vestan interior at magmatic temperatures is expected to be negligible, the weighted average δD value for Stannern clinopyroxenes is our best estimate of the δD of their mantle source on 4 Vesta. This value is lower than any known cometary composition (Alexander et al., 2018). It is also lower than the average δD value for bulk carbonaceous (CI, CM, CV, and CO) chondrites (Alexander et al., 2012), Earth's depleted upper mantle (Clog et al., 2013) and other terrestrial aqueous reservoirs (Hoefs, 2015) (Fig. 6).

4.4. Water content of bulk silicate 4 Vesta

Several recent studies have shown that the compositions of clinopyroxene phenocrysts in terrestrial igneous rocks can be used to reliably estimate magmatic water contents (Aubaud et al., 2004; O'Leary et al., 2010; Wade et al., 2008; Warren and Hauri, 2014; Hauri et al., 2006; Weis et al., 2018). As noted previously in Sections 4.1 and 4.3 above, the clinopyroxenes in the relatively equilibrated eucrites such as Juvinas and Tirhert have likely undergone subsolidus H^+ diffusion due to thermal metamorphism to a greater degree than this mineral in less equilibrated eucrites such as Stannern. Therefore, we assume that the measured H_2O content in the clinopyroxene with the highest Mg# (i.e., Pyroxene 1a with 9.7 ± 1.9 μg/g H_2O; Tables 1 and S1) of Stannern most closely approximates the original water abundance in first-formed clinopyroxenes in equilibrium with their parent magma.

Previous work has described a linear relation between clinopyroxene-silicate melt partition coefficient for H_2O and the amount of tetrahedral Al^{3+} in the clinopyroxene (O'Leary et al., 2010; Wade et al., 2008; Weis et al., 2018). However, the parameterization of the clinopyroxene-melt partition coefficient corresponds to higher pressure (i.e., 1.5 GPa) than expected for an asteroidal body such as 4 Vesta. Recently, Sarafian et al. (2019) determined a partition coefficient for H_2O (i.e., D = 0.1) between pyroxene and melt at low pressure (0.1 MPa) and low water content (200 μg/g). These authors acknowledged that one caveat of their experiments is the drastic difference in oxygen fugacity between their experimental melt and eucritic melts, which crystallized at about 5 log units lower (i.e. $\Delta IW \sim -2.2$ for Vesta, Righter and Drake, 1996). Although oxygen fugacity is known to affect the H speciation in melt (Newcombe et al., 2017), Sarafian et al. (2019)

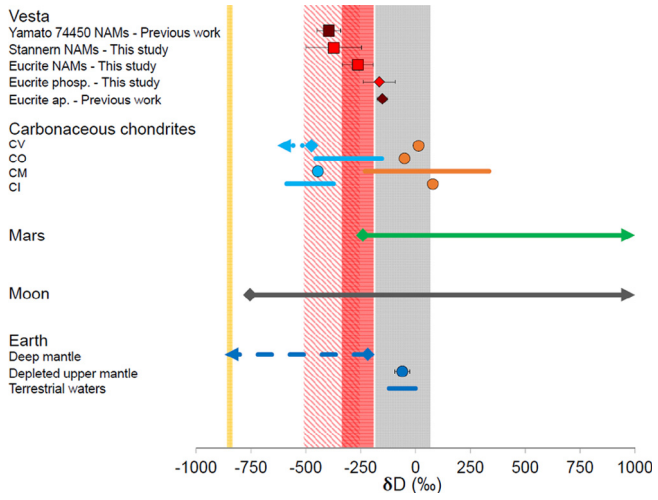

Fig. 6. The δD distribution in the inner Solar System. The two red squares and vertical bands show our estimates of the δD value for 4 Vesta: the vertical solid red band represents our upper limit estimate of the δD value for 4 Vesta (–263 ± 70‰; weighted average, with 2SD errors, of the δD values of clinopyroxenes in Juvinas, Stannern, and Tirhert) and the vertical diagonally-striped red band represents our best estimate of the δD value for 4 Vesta based solely on Stannern NAMs (–373 ± 127‰; weighted average, with 2SD errors, of the δD values of clinopyroxenes in Stannern). Also shown is the weighted average, with 2SD errors, of phosphates (phosp.) reported in this study (red diamond). For comparison, the weighted average of eucritic apatites (ap.), with 2SD errors, from the combined data sets of Sarafian et al. (2014) and Barrett et al. (2016) is also showed (maroon diamond), as well as the minimally spallation corrected δD value of Yamato 74450 pyroxene reported by Sarafian et al. (2019) (maroon square). The vertical gray band represents the weighted average δD with 2SD error of bulk carbonaceous (CI, CM, CO, CV) chondrites (–61 ± 120‰; calculated from the compiled dataset in Alexander et al., 2012); the δD values of measured bulk samples (orange) and those estimated for water (light blue) from different carbonaceous chondrite types are also shown (Alexander et al., 2012). The dark gray and green arrows indicate the large range in δD reported previously in lunar samples and martian meteorites (Tartèse et al., 2013; Robinson et al., 2016; Barnes et al., 2014; Gillet et al., 2002; Mane et al., 2016; Usui et al., 2012). The lowest lunar values were reported by Robinson et al. (2016) and Barnes et al. (2014), and the lowest Martian values by Gillet et al. (2002). For Earth, the values for deep mantle (Hallis et al., 2015) and depleted upper mantle (Clog et al., 2013) are shown; dashed blue arrow represents the estimated upper limit for the deep mantle reservoir and the dark blue line represents the range of δD values for terrestrial water reservoirs (Hoefs, 2015). The δD value for the protosolar nebula (vertical yellow band) is from Geiss and Gloeckler (1998). (For interpretation of the references to color in this figure legend, the reader is referred to the web version of this article.)

argued that the difference in H speciation between eucritic melts and their experimental melts should not be considerably different. On the other hand, it has been shown that H incorporation in NAMs is strongly dependent on the pressure (Demouchy and Bolfan-Casanova, 2016; and references therein). Since the partition coefficient for H_2O recently reported by Sarafian et al. (2019) was determined at low pressure, it is currently the most appropriate value available for conditions on asteroid 4 Vesta. Using this new partition coefficient, the H_2O content of the eucrite parent melt in equilibrium with the earliest-formed Stannern clinopyroxene with the highest Mg# (i.e., 9.7 ± 1.9 μg/g H_2O; Table 1) is estimated to be between 78 and 116 μg/g. This estimate is higher compared to that of Sarafian et al. (2019) (i.e., 50–70 μg/g).

Previous studies have suggested that eucrites were formed as either partial melts or residual melts after extensive melting and fractional crystallization processes on their parent body (e.g., Stolper, 1977; Ikeda and Takeda, 1985; Yamaguchi et al., 2009; Mandler and Elkins-Tanton, 2013; Ashcroft and Wood, 2015). In either case, the silicate fraction of their source region (presumably 4 Vesta) is required to have undergone 80–85% solidification prior to the formation of eucrite magmas (Mandler and Elkins-Tanton, 2013). Using the eucrite parent magma water content estimated here (i.e., 78 to 116 μg/g H_2O), a mass balance calculation assuming that, to first order, the solidified fraction was anhydrous, the H_2O content of the bulk silicate reservoir for 4 Vesta is estimated to be ~12–23 μg/g. This is similar to the range of 10–70 μg/g H_2O estimated by Sarafian et al. (2019) for the Vestan mantle. This estimate is significantly lower than that for the present day bulk silicate Earth (i.e., 1000–3000 μg/g H_2O (Marty, 2012); 1100 ± 220 μg/g H_2O (Palme and O'Neil, 2014); ~3900 μg/g H_2O (Peslier et al., 2017; and references therein)), and is similar to the lower end of the range of water contents estimated for the bulk silicate Moon (~1 to ~450 μg/g H_2O; McCubbin et al., 2010; Hauri et al., 2011, 2015; Hui et al., 2013; Tartèse et al., 2013; Füri et al., 2014; Chen et al., 2015). As also noted by Sarafian et al. (2019), the range of water abundances for the bulk silicate reservoir for 4 Vesta estimated here is likely to be a lower limit due to the potential for Magma Ocean degassing, degassing from the eucrite parent melt during eruption, and/or some diffusional loss of hydrogen from the Stannern pyroxene.

5. ASTEROID 4 VESTA'S WATER SOURCE AND IMPLICATIONS FOR THE INNER SOLAR SYSTEM

The D-poor mantle reservoir for 4 Vesta implied by the δD analyses reported here for eucritic clinopyroxenes is consistent with that proposed recently for Earth's deep

mantle reservoir (δD < –218‰; Hallis et al., 2015) (Fig. 6). Previously reported δD values in planetary materials derived from the Moon and Mars span a wide range (from as low as the values for eucritic clinopyroxenes reported here, up to several thousands of per mil; Fig. 6) and have been attributed to a variety of processes (Sarafian et al., 2014 and references therein). Although some authors have made the case that the mantles of the Moon and Mars have δD values similar to bulk carbonaceous chondrites (e.g., Saal et al., 2013; Füri et al., 2014; Mane et al., 2016), there are still significant uncertainties in the assumptions for these estimates. We note, however, that some studies have suggested the presence of a highly D-poor reservoir in the lunar interior (Robinson et al., 2016; Barnes et al., 2014, Desch and Robinson, 2019) as well as D-poor reservoir in the mantle of Mars (Gillet et al., 2002). Therefore, it is possible that it is not just the interior of 4 Vesta that is characterized by a δD value lower than bulk carbonaceous chondrites, but that D-poor reservoirs are more common in other rocky bodies in the inner Solar System.

It has previously been argued that to account for the δD value represented by bulk carbonaceous chondrites and the Earth's upper mantle it was necessary to import D-enriched water ice from the coldest outer regions of the disk (Drouart et al., 1999; Cleeves et al., 2014). This was because the δD value of nebular water cannot reach chondritic values (~0‰) by simple equilibrium isotopic exchange between gaseous H_2O and protosolar H_2 at a terrestrial distance from the Sun (Lécluse and Robert, 1994) or by irradiation of silicate dust precursors having an initially protosolar δD (Roskosz et al., 2016). Moreover, models involving the simple degassing and Rayleigh fractionation of the protosolar nebula (similar to that described in Sarafian et al., 2014) cannot account for the combined hydrogen, carbon, and nitrogen isotope compositions of inner Solar System bodies. However, our best estimates of the δD value for the Vestan mantle (with an upper limit of –263 ± 70‰, and likely close to –371 ± 127‰) overlap with values estimated for water from several types of carbonaceous chondrites (Alexander et al., 2012; Piani et al., 2018; Fig. 6). Bulk chondritic values, which typically have somewhat higher δD (Fig. 6), are then attributed to hydrogen isotopic exchange between a D-poor water reservoir with D-rich organics in a closed system (Alexander et al., 2012; Piani et al., 2018). It was shown recently that kinetic isotopic exchange between gaseous H_2O in the nebula and protosolar H_2 can account for the D-poor water reservoir of CM carbonaceous chondrites (Piani et al., 2018; and references therein). Such a D-poor water reservoir, which is similar to that suggested here for the mantle of 4 Vesta, could then have supplied bodies in the inner Solar System with their water inventory. In this case, however, this D-poor water reservoir would reside in the nebula as gas or in the solid phase as ice (but without the associated D-rich organics found in carbonaceous chondrites) and would need to be incorporated into planetesimals such as 4 Vesta at its time of accretion. Indeed, chondritic abundances of highly siderophile elements in diogenites argue for influx of 0.01–1.5% of chondritic material to 4 Vesta after its core formation (2–3 Ma after CAI formation), that might have been heterogeneously distributed in the mantle of 4 Vesta (Day et al., 2012; Dale et al., 2012). It is thus difficult to assess to what extent this late chondritic accretion on 4 Vesta would be reflected in its δD composition. It is also possible that 4 Vesta, which may have been close to the snow line at the time of its accretion in the early Solar System, may have acquired its D-poor composition from the accretion of light nebular water ice similar to the water component identified in carbonaceous chondrites.

Ingassing of an early, dense nebular atmosphere (containing such components as H_2 and H_2O) has been proposed as a means of acquiring volatiles and a D-poor signature in the interiors of larger planetary bodies like Earth (Wu et al., 2018; Sharp, 2017; Hirschmann et al., 2012), as well as Theia, the embryo that formed the Moon (Desch and Robinson, 2019). The protosolar H_2 could also have been incorporated into the growing Earth by direct dissolution in an early magma ocean (Yang et al., 2016). Subsequent outgassing could then elevate δD to a somewhat higher value due to preferential H loss (e.g., 95–99% H loss starting from a nebular-like δD value would result in a δD of ~−300‰; Sharp, 2017). However, while such processes may indeed have contributed to the volatile budget and influenced D/H ratios of larger planetary bodies (i.e. >0.3 M_E) which were able to accrete a thin atmosphere of nebular H_2 (Desch and Robinson, 2019), it is unlikely that these processes were significant for a planetesimal such as 4 Vesta, with a mass of 4.3×10^{-5} M_E (Sharp, 2017). One possibility for the incorporation of a D-poor signature into planetesimals (and planetary bodies) from nebular gas could be the chemisorption of nebular OH on forsterite surfaces during condensation of this mineral from the nebula prior to accretion of planetesimals (Asaduzzaman et al., 2015).

Finally, while the exact mechanism by which the interior of 4 Vesta, and possibly other bodies in the inner Solar System, acquired a D-poor composition is unclear, it is likely that it occurred early during accretion, either prior to a magma ocean phase or in the early stages of a magma ocean. Depending on the specific mechanism involved, and whether or not the initial H-bearing reservoir was fractionated by subsequent processes (for instance, D-enrichment due to hydrogen loss during the heating associated with accretionary growth of planetary bodies), the relatively D-poor composition proposed here in the interior of 4 Vesta (and possibly other bodies in the inner Solar System) does not necessarily preclude later addition of asteroidal or cometary material that may be required to meet dynamical (Morbidelli et al., 2000; O'Brien et al., 2018) and geochemical (Dale et al., 2012; Day et al., 2012) constraints.

Declaration of Competing Interest

The authors declare that they have no known competing financial interests or personal relationships that could have appeared to influence the work reported in this paper.

ACKNOWLEDGMENTS

We thank three anonymous reviewers for their very detailed but constructive comments, all of which helped improve substantially the quality of this manuscript, as well as Jeffrey G. Catalano and James Day for efficient editor handling. This work was partly supported by the NASA Solar System Workings grant NNX16AT37G to M.W. and a STFC grant #ST/P000657/1 to M.A. and I.A.F. We acknowledge NSF EAR 1352996 for support of the ASU SIMS facility. The meteorite samples studied here were obtained from the collection in the Center for Meteorite Studies at ASU. We thank the Department of Mineral Sciences at the Smithsonian institution, and L. Hale, for the pyroxene standards. This project has received funding from the European Union's Horizon 2020 research and innovation programme under the Marie Skłodowska-Curie grant agreement no. 884029.

APPENDIX A. SUPPLEMENTARY MATERIAL

Supplementary data to this article can be found online at https://doi.org/10.1016/j.gca.2021.01.004.

REFERENCES

Albarède F. (2009) Volatile accretion history of the terrestrial planets and dynamic implications. *Nature* **461**, 1227–1233.

Alexander C. M. O'D., Bowden R., Fogel M. L., Howard K. T., Herd C. D. K. and Nittler L. R. (2012) The provenances of asteroids, and their contributions to the volatile inventories of the terrestrial planets. *Science* **337**, 721–723.

Alexander C. M. O'D., McKeegan K. D. and Altwegg K. (2018) Water reservoirs in small planetary bodies: Meteorites, Asteroids, and comets. *Space Sci. Rev.* **214**(1), 36.

Asaduzzaman A., Muralidharan K. and Ganguly J. (2015) Incorporation of water into olivine during nebular condensation: Insights from density functional theory and thermodynamics, and implications for phyllosilicate formation and terrestrial water inventory. *Meteorit. Planet. Sci.* **50**(4), 578–589.

Ashcroft H. O. and Wood B. J. (2015) An experimental study of partial melting and fractional crystallization on the HED parent body. *Meteorit. Planet. Sci.* **50**, 1912–1924.

Aubaud C., Hauri E. H. and Hirschmann M. M. (2004) Hydrogen partition coefficients between nominally anhydrous minerals and basaltic melts. *Geophys. Res. Lett.* **31**, L20611.

Aubaud C., Withers A., Hirschmann M., Guan Y., Leshin Y., Mackwell S. and Bell D. (2007) Intercalibration of FTIR and SIMS for hydrogen measurements in glasses and nominally anhydrous minerals. *Am. Mineral.* **92**, 811–828.

Barnes J. J., Tartèse R., Anand M., McCubbin F. M., Franchi I. A., Starkey N. A. and Russell S. S. (2014) The origin of water in the primitive Moon as revealed by the lunar highlands samples. *Earth Planet. Sci. Lett.* **390**, 244–252.

Barnes J. J., Franchi I. A., McCubbin F. M. and Anand M. (2019) Multiple volatile reservoirs in the lunar interior revealed by the isotopic composition of chlorine in lunar basalts. *Geochim. Cosmochim. Acta* **206**, 144–162.

Barrat J. A., Blichert-Toft J., Gillet P. H. and Keller F. (2000) The differentiation of eucrites: the role of in situ crystallization. *Meteorit. Planet. Sci.* **35**, 1087–1100.

Barrat J.-A. (2004) Determination of parental magmas of HED cumulates: the effectsof interstitial melts. *Meteorit. Planet. Sci.* **39**, 1767–1779.

Barrat J. A., Yamaguchi A., Greenwood R. C., Bohn M., Cotton J., Benoit M. and Franchi I. A. (2007) The Stannern trend eucrites: contamination of main group eucriticmagmas by crustal partial melts. *Geochim. Cosmochim. Acta* **71**, 4108–4124.

Barrat J. A., Yamaguchi A., Bunch T. E., Bohn M., Bollinger C. and Ceuleneer G. (2011) Possible fluid–rock interactions on differentiated asteroids recorded in eucritic meteorites. *Geochim. Cosmochim. Acta* **75**, 3839–3852.

Barrett T. J., Barnes J. J., Tartèse R., Anand M., Franchi I. A., Greenwood R. C., Charlier B. L. A. and Grady M. M. (2016) The abundance and isotopic composition of water in eucrites. *Meteorit. Planet. Sci.* **105**, 146–171.

Barrett T. J., Barnes J. J., Anand M., Franchi I. A., Greenwood R. C., Charlier B. L. A., Zhao X., Moynier F. and Grady M. M. (2019) Investigating magmatic processes in the early Solar System using the Cl isotopic systematics of eucrites. *Geochim. Cosmochim. Acta* **266**, 582–597.

Bell D. R., Ihinger P. D. and Rossman G. R. (1995) Quantitative analysis of trace OH in garnet and pyroxenes. *Am. Mineral.* **80**, 465–474.

Bell D. R. and Ihinger P. D. (2000) The isotopic composition of hydrogen in nominally anhydrous mantle minerals. *Geochim. Cosmochim. Acta* **64**, 2109–2118.

Bindeman I. N., Kamenetsky V. S., Palandri J. and Vennemann T. (2012) Hydrogen and oxygen isotope behaviors during variable degrees of upper mantle melting: Example from the basaltic glasses from Macquarie Island. *Chem. Geol.* **310–311**, 126–136.

Bindeman I. N., Lundstrom C. C., Bopp C. and Huang F. (2013) Stable isotope fractionation by thermal diffusion through partially molten wet and dry silicate rocks. *Earth Planet. Sci. Lett.* **365**, 51–62.

Boyce J. W., Tomlinson S. M., McCubbin F. M., Greenwood J. P. and Treiman A. H. (2014) The lunar apatite paradox. *Science* **344**, 400–402.

Chen Y., Zhang Y., Liu Y., Guan Y., Eiler J. and Stolper E. M. (2015) Water, fluorine, and sulfur concentrations in the lunar mantle. *Earth Planet. Sci. Lett.* **427**, 37–46.

Cleeves L. I., Bergin E. A., Alexander C. M. O'D., Du F., Graninger D., Öberg K. I. and Harries T. M. (2014) The ancient heritage of water ice in the solar system. *Science* **345** (6204), 1590–1593.

Clog M., Aubaud L., Cartigny P. and Dosso L. (2013) The hydrogen isotopic composition and water content of southern Pacific MORB: A reassessment of the D/H ratio of the depleted mantle reservoir. *Earth Planet. Sci. Lett.* **381**, 156–165.

Dale C. W., Burton K. W., Greenwood R. C., Gannoun A., Wade J., Wood B. J. and Pearson D. G. (2012) Late accretion on the earliest planetesimals revealed by the highly siderophile elements. *Science* **336**(6077), 72–75.

Day J. M. D., Walker R. J., Qin L. and Rumble, III, D. (2012) Late accretion as a natural consequence of planetary growth. *Nature Geosciences* **5**, 614–617.

Day J. M. D. and Moynier F. (2014) Evaporative fractionation of volatile stable isotopes and their bearing on the origin of the Moon. *Phil. Trans. R. Soc. A* **372**, 20130259.

Demouchy S. and Bolfan-Casanova N. (2016) Distribution and transport of hydrogen in the lithospheric mantle: A review. *Lithos* **240–243**, 402–425.

Desch S. J. and Robinson K. L. (2019) A unified model for hydrogen in Earth and Moon: No one expects the Theia contribution. *Geochemistry* **79**, 125546.

Drouart A., Dubrulle B., Gautier D. and Robert F. (1999) Structure and transport in the solar nebula from constraints on deuterium enrichment and giant planets formation. *Icarus* **140**(1), 129–155.

Füri E., Deloule E., Gurenko A. and Marty B. (2014) New evidence for chondritic lunar water from combined D/H and noble gas analyses of single Apollo 17 volcanic glasses. *Icarus* **229**, 109–120.

Füri E., Deloule E. and Trappitsch R. (2017) The production rate of cosmogenic deuterium at the Moon's surface. *Earth Planet. Sci. Lett.* **474**, 76–82.

Geiss J. and Gloeckler G. (1998) Abundances of deuterium and helium-3 in the protosolar cloud. *Space Sci. Rev.* **84**, 239–250.

Gillet P., Barrat J. A., Deloule E., Wadhwa M., Jambon A., Sautter V., Devouard B., Neuville D., Benzerara K. and Lesourd M. (2002) Aqueous alteration in the Northwest Africa 817 (NWA 817) Martian meteorite. *Earth Planet. Sci. Lett.* **203**, 431–444.

Halliday A. N. (2013) The origins of volatiles in the terrestrial planets. *Geochim. Cosmochim. Acta* **75**, 3839–3852.

Hallis L. J., Huss G. R., Nagashima K., Taylor G. J., Halldo´rsson S. A., Hilton D. R., Mottl M. J. and Meech K. J. (2015) Evidence for primordial water in Earth's deep mantle. *Science* **350**, 795–797.

Hagemann F., Nief G. and Roth E. (1970) Absolute isotopic scale for deuterium analyses of natural waters. Absolute D/H ratio for SMOW. *Tellus* **22**(6), 712–715.

Hauri E. H., Wang J., Dixon J. E., King P. L., Mandeville C. and Newman S. (2002) SIMS analysis of volatiles in silicate glasses: 1. Calibration, matrix effects and comparisons with FTIR. *Chem. Geol.* **183**(1–4), 99–114.

Hauri E. H., Gaetani G. A. and Green T. H. (2006) Partitioning of water during melting of the Earth's upper mantle at H_2O-undersaturated conditions. *Earth Planet. Sci. Lett.* **248**, 715–734.

Hauri E. H., Weinreich T., Saal A. E., Rutherford M. C. and Van Orman J. A. (2011) High pre-eruptive water contents preserved in lunar melt inclusions. *Science* **333**, 213–215.

Hauri E. H., Saal A. E., Rutherford M. J. and Van Orman J. A. (2015) Water in the Moon's interior: Truth and consequences. *Earth Planet. Sci. Lett.* **409**, 252–264.

Hirschmann M. M., Withers A. C., Ardia P. and Foley N. T. (2012) Solubility of molecular hydrogen in silicate melts and consequences for volatile evolution of terrestrial planets. *Earth Planet. Sci. Lett.* **345**, 38–48.

Hoefs J. (2015) Variations of stable isotope ratios in nature. *Stable Isotope Geochemistry*. Springer, Switzerland.

Hopkins M. D., Mojzsis S. J., Bottke W. F. and Abramov O. (2015) Micrometer-scale U-Pb age domains in eucrite zircons, impact re-setting, and the thermal history of the HED parent body. *Icarus* **245**, 367–378.

Hsu W. and Crozaz G. (1996) Mineral chemistry and the petrogenesis of eucrites: I.Noncumulate eucrites. *Geochim. Cosmochim. Acta* **60**, 4571–4591.

Hui H., Peslier A. H., Zhang Y. and Neal C. R. (2013) Water in lunar anorthosites and evidence for a wet early Moon. *Nat. Geosci.* **6**, 177–180.

Hutchison R. (2004) *Meteorites: A Petrologic, Chemical and Isotopic Synthesis*. Cambridge University Press.

Iizuka T., Yamaguchi A., Haba M. K., Amelin Y., Holden P., Zink S., Huyskens M. and Ireland T. R. (2015) Timing of global crustal metamorphism on Vesta as revealed by high-precision U-Pb dating and trace element chemistry of eucrite zircon. *Earth Planet. Sci. Lett.* **409**, 182–192.

Ikeda Y. and Takeda H. (1985) A model for the origin of basaltic achondrites based on the Yamato 7308 howardite. *J. Geophys. Res.* **90**, C649–C663.

Jolliff B. L., Hughes J. M., Freeman J. J. and Zeigler R. A. (2006) Crystal chemistry of lunar merrillite and comparison to other meteoritic and planetary suites of whitlockite and merrillite. *Am. Mineral.* **91**, 1583–1595.

Karner J., Papike J. J. and Shearer C. K. (2004) Plagioclase from planetary basalts: chemical signatures that reflect planetary volatile budgets, oxygen fugacity, and styles of igneous differentiation. *Am. Mineral.* **89**, 1101–1109.

Kleine T., Mezger K., Palme H., Scherer E. and Münker C. (2005) The W isotope composition of eucrite metals: constraints on the timing and cause of the thermal metamorphism of basaltic eucrites. *Earth Planet. Sci. Lett.* **231**, 41–52.

Kleine T. and Wadhwa M. (2017) Chronology of planetesimal differentiation. In *Chronology of Planetesimal Differentiation*. Cambridge University Press, pp. 224–245.

Koga K., Hauri E. H., Hirschmann M. and Bell D. (2003) Hydrogen concentration analyses using SIMS and FTIR: comparisons and calibration for nominally anhydrous minerals. *Geochem. Geophys. Geosyst.* **4**(2).

Kumamoto K. M., Warren J. M. and Hauri E. H. (2017) New SIMS reference materials for measuring water in upper mantle minerals. *Am. Mineral.* **102**, 537–547.

Kyser T. K. and O'Neill J. R. (1984) Hydrogen isotope systematics of submarine basalts. *Geochim. Cosmochim. Acta* **106**, 71–83.

Kyser T. K., Lesher C. E. and Walker D. (1998) The effects of liquid immiscibility and thermal diffusion on oxygen isotopes in silicate liquids. *Contrib. Miner. Petrol.* **133**, 373–381.

Lécluse C. and Robert F. (1994) Hydrogen isotope exchange reaction rates: origin of water in the inner solar system. *Geochim. Cosmochim. Acta* **58**(13), 2927–2939.

Lécuyer C., Gillet P. and Robert F. (1998) The hydrogen isotope composition of seawater and the global water cycle. *Chem. Geol.* **145**, 249–261.

Liu Y., Guan Y., Zhang Y., Rossman G. R., Eiler J. M. and Taylor L. A. (2012) Direct measurement of hydroxyl in the lunar regolith and the origin of lunar surface water. *Nat. Geosci.* **5** (11), 779–782.

Mandler B. E. and Elkins-Tanton L. T. (2013) The origin of eucrites, diogenites, and olivine diogenites: Magma ocean crystallization and shallow magma chamber processes on Vesta. *Meteorit. Planet. Sci.* **48**(11), 2333–2349.

Mane P., Hervig R., Wadhwa M., Garvie L. A. J., Balta J. B. and McSween H. Y. (2016) Hydrogen isotopic composition of the Martian mantle inferred from the newest Martian meteorite fall, Tissint. *Meteorit. Planet. Sci.* **51**, 2073–2091.

Mayne R. G., McSween, Jr., H. Y., McCoy T. J. and Gale A. (2009) Petrology of the unbrec-ciated eucrites. *Geochim. Cosmochim. Acta* **73**, 794–819.

Marty B. (2012) The origins and concentrations of water, carbon, nitrogen and noble gases on Earth. *Earth Planet. Sci. Lett.* **313–314**, 56–66.

Mathez E. A. and Webster J. D. (2005) Partitioning behavior of chlorine and fluorine in the system apatite-silicate melt-fluid. *Geochim. Cosmochim. Acta* **69**(5), 1276–1286.

McCubbin F., Steele A., Hauri E. H., Nekvasil H., Yamashita S. and Hemley R. J. (2010) Nominally hydrous magmatism on the Moon. *Proc. Natl. Acad. Sci. U. S. A.* **107**(25), 11223–11228.

McCubbin F. M., Vander Kaaden K. E., Tartèse R., Klima R. L., Liu Y., Mortimer J., Barnes J. J., Shearer C. K., Treiman A. H., Lawrence D. J., Elardo S. M., Hurley D. M., Boyce J. W. and Anand M. (2015a) Magmatic volatiles (H, C, N, F, S, Cl) in the lunar mantle, crust, and regolith: Abundances, distributions, processes, and reservoirs. *Am. Mineral.* **100**, 1668–1707.

McCubbin F. M., Vander Kaaden K. E., Tartèse R., Boyce J. W., Mikhail S., Whitson E. S., Bell A. S., Anand M., Franchi I. A., Wang J. and Hauri E. H. (2015b) Experimental investigation of F, Cl, and OH partitioning between apatite and Fe-rich basaltic

melt at 1.0–1.2 GPa and 950–1000 °C. *Am. Mineral.* **100**, 1790–1802.

McSween H. Y., Mittlefehldt D. W., Beck A. W., Mayne R. G. and McCoy T. J. (2011) HED meteorites and their relationship to the geology of Vesta and the Dawn mission. *Space Sci. Rev.* **163** (1), 141–174.

Merlivat L., Lelu M., Nief G. and Roth E. (1976) Spallation deuterium in rock 70215. In *Proceeding of the Lunar Science Conference*, 7, pp. 649–658. Proceeding of the Lunar Science Conference.

Metzler K., Bobe K. D., Palme H., Spettel B. and Stöffler D. (1995) Thermal and impact metamorphism on the HED parent asteroid. *Planet. Space Sci.* **43**, 499–525.

Mittlefehldt D. W. and Lindstrom M. M. (2003) Geochemistry of eucrites: Genesis of basaltic eucrites, and Hf and Ta as petrogenetic indicators for altered antarctic eucrites. *Geochim. Cosmochim. Acta* **67**(10), 1911–1935.

Mittlefehldt D. W. (2015) Asteroid (4) Vesta: I. The howardite-eucrite-diogenite (HED) clan of meteorites. *Chem. Erde* **75**, 155–183.

Morbidelli A., Chambers J., Lunine J. I., Petit J. M., Robert F., Valsecchi G. B. and Cyr K. E. (2000) Source regions and timescales for the delivery of water to the Earth. *Meteorit. Planet. Sci.* **35**, 1309–1320.

Mosenfelder J. L., Le Voyer M., Rossman G. R., Guan Y., Bell D. R., Asimow P. D. and Eiler J. M. (2011) Analysis of hydrogen in olivine by SIMS: evaluation of standards and protocol. *Am. Mineral.* **96**, 1725–1741.

Newcombe M. E., Brett A., Beckett J. R., Baker M. B., Newman S., Guan Y., Eiler J. M. and Stolper E. M. (2017) Solubility of water in lunar basalt at low pH_2O. *Geochim. Cosmochim. Acta* **200**, 330–352.

Nyquist L. E., Takeda H., Bansal B. M., Shih C.-Y., Wiesmann H. and Wooden J. L. (1986) Rb-Sr and Sm-Nd internal isochron ages of a subophitic basalt clast and a matrix sample from the Y75011 eucrite. *J. Geophys. Res.* **91**(B8), 8137–8150.

O'Brien D. P., Izidoro A., Jacobson S. A., Raymond S. N. and Rubie D. C. (2018) The delivery of water during terrestrial planet formation. *Space Sci. Rev.* **214**, 47.

O'Leary J. A., Gaetani G. H. and Hauri E. H. (2010) The effect of tetrahedral Al^{3+} on the partitioning of water between clinopyroxene and silicate melt. *Earth Planet. Sci. Lett.* **297**, 111–120.

Palme H. and O'Neil H. S. C. (2014) Cosmochemical estimates of mantle composition. *Treatise Geochem.*, 1–39.

Piani L., Yurimoto H. and Remusat L. (2018) A dual origin for water in carbonaceous asteroids revealed by CM chondrites. *Nat. Astron* **2**, 317–323.

Piani L., Marrocchi Y., Rigaudier T., Vacher L. G., Thomassin D. and Marty B. (2020) Earth's water may have been inherited from material similar to enstatite chondrite meteorites. *Science* **369**(6507), 1110–1113.

Pichavant, M., Verrera, J.V., Boulmer, S., Brique, L. Joron, J.L., Juteau, M., Marin, L., Michard, A., Sheppard, S.M.F., Treuil, M., Vernet, M., 1987. The Macusanite glasses, SE Peru: evidence of chemical fractionation in peraluminous magmas. In: Mysen B.O. (Ed.), Magmatic Processes: Physicochemical Principles, Geochemical Society Special Publication, 1, 359–373.

Peslier A. H., Schönbächler M. and Busemann H. (2017) Water in the Earth's interior: distribution and origin. *Space Sci. Rev.* **212**, 743–811.

Prettyman T. H., Mittlefehldt D. W., Yamashita N., Lawrence D. J., Beck A. W., Feldman W. C., McCoy T. J., McSween H. Y., Toplis M. J., Titus T. N., Tricarico P., Reedy R. C., Hendricks J. S., Forni O., Le Corre L., Li J.-Y., Mizzon H., Reddy V., Raymond C. A. and Russell C. T. (2012) Elemental Mapping by Dawn Reveals Exogenic H in Vesta's Regolith. *Science* **338** (6104), 242–246.

Pringle E. and Moynier F. (2017) Rubidium isotopic composition of the Earth, meteorites, and the Moon: evidence for the origin of volatile loss during planetary accretion. *Earth Planet. Sci. Lett.* **473**, 62–70.

Pun A. and Papike J. (1996) Unequilibrated eucrites and the equilibrated Juvinas eucrite: Pyroxene REE systematics and major, minor, and trace element zoning. *Am. Mineral.* **81**, 1438–1451.

Righter K. and Drake M. J. (1996) Core formation in Earth's Moon, Mars and Vesta. *Icarus* **124**, 513–529.

Righter, K., Garber, J., 2011. The HED Compendium. Johnson Space Center, Houston, TX. http://curator.jsc.nasa.gov/antmet/hed/.

Robert F. (2003) The D/H ratio in chondrites. *Space Sci. Rev.* **106**, 87–101.

Robinson K. L., Barnes J. J., Nagashima K., Thomen A., Franchi I. A., Huss G. R., Anand M. and Taylor G. J. (2016) Water in evolved lunar rocks: Evidence for multiple reservoirs. *Geochim. Cosmochim. Acta* **188**, 244–260.

Roskosz M., Laurent B., Leroux H. and Remusat L. (2016) Experimental investigation of irradiation-driven hydrogen isotope fractionation in analogs of protoplanetary hydrous silicate dust. *Astrophys. J.* **832**, 55–66.

Roskosz M., Deloule E., Ingrin J., Depecker C., Laporte D., Merkel S., Remusat L. and Leroux H. (2018) Kinetic D/H fractionation during hydration and dehydration of silicate glasses, melts and nominally anhydrous minerals. *Geochim. Cosmochim. Acta* **233**, 14–32.

Russell C. T., Raymond C. A., Jaumann R., McSween H. Y., De Sanctis M. C., Nathues A., Prettyman T. H., Ammannito E., Reddy V., Preusker F., O'Brien D. P., Marchi S., Denevi B. W., Buczkowsk D. L., Pieters C. M., McCord T. B., Li J. Y., Mittlefehldt D. W., Combe J. P., Williams D. A., Hiesinger H., Yingst R. A., Polanskey C. A. and Joy S. P. (2013) Dawn completes its mission at 4 Vesta. *Meteorit. Planet. Sci.* **48**(11), 2076–2089.

Ruzicka A., Grossman J., Bouvier A. and Agee C. B. (2015) The meteoritical bulletin N°103. *Meteorit. Planet. Sci.* **52**, 5.

Saal A. E., Hauri E. H., Van Orman J. A. and Rutherford M. J. (2013) Hydrogen isotopes in lunar volcanic glasses and melt inclusions reveal a carbonaceous chondrite heritage. *Science* **340**(6138), 1317–1320.

Saccocia P. J., Seewald J. S. and Shanks, III, W. C. (2009) Oxygen and hydrogen isotope fractionation in serpentine-water and talc-water systems from 250 to 450 C, 50 MPa. *Geochim. Cosmochim. Acta* **73**, 6789–6804.

Sarafian A. R., Nielsen S. G., Marschall H. R., McCubbin F. M. and Monteleone B. D. (2014) Early accretion of water in the inner solar system from a carbonaceous chondrite-like source. *Science* **346**, 623–626.

Sarafian A. R., John T., Roszjar J. and Whitehouse M. J. (2017) Chlorine and hydrogen degassing in Vesta's magma ocean. *Earth Planet. Sci. Lett.* **459**, 311–319.

Sarafian A. R., Nielsen S. G., Marschall H. R., Gaetani G. A., Righter K. and Berger E. L. (2019) The water and fluorine content of 4 Vesta. *Geochim. Cosmochim. Acta* **266**, 568–581.

Sharp Z. D. (2017) Nebular ingassing as a source of volatiles to the terrestrial planets. *Chem. Geol.* **448**, 137–150.

Singer J. A., Greenwood J. P., Itoh S., Sakamoto N. and Yurimoto H. (2017) Evidence for the solar wind in lunar magmas: A study of slowly cooled samples of the Apollo 12 olivine basalt suite. *Geochem. J.* **51**, 95–104.

Skogby H. (2006) Water in Natural Mantle Minerals I: Pyroxenes. *Rev. Mineral. Geochem.* **62**, 155–167.

Stephant A. and Robert F. (2014) The negligible chondritic contribution in the lunar soils water. *Proc. Natl. Acad. Sci.* **111**(42), 15007–15012.

Stephant A., Garvie L., Mane P., Hervig R. and Wadhwa M. (2018) Terrestrial exposure of a fresh Martian meteorite causes rapid changes in hydrogen isotopes and water concentrations. *Nat. Sci. Rep.* **8**, 12385. https://doi.org/10.1038/s41598-018-30807-w.

Stephant A., Anand M., Tartèse R., Zhao X., Degli-Alessandrini G. and Franchi I. A. (2020) The hydrogen isotopic composition of lunar melt inclusions: An interplay of complex magmatic and secondary processes. *Geochim. Cosmochim. Acta* **284**, 196–221.

Stolper E. (1977) Experimental petrology of eucritic meteorites. *Geochim. Cosmochim. Acta* **41**, 587–611.

Strashnov I., Bland P. A., Spurny P., Towner M. C. and Gilmour J. D. (2013) Times of impacts that deliver samples of Vesta to Earth derived from ultrasensitive ^{81}Kr–Kr cosmic ray exposure age analysis of eucrites. *Geochim. Cosmochim. Acta* **106**, 71–83.

Takeda H. and Graham A. L. (1991) Degree of equilibration of eucritic pyroxenes and thermal metamorphism of the earliest planetary crust. *Meteoritics* **26**, 129–134.

Tartèse R. et al. (2013) The abundance, distribution, and isotopic composition of hydrogen in the Moon as revealed by basaltic lunar samples: implications for the volatile inventory of the Moon. *Geochim. Cosmochim. Acta* **122**, 58–74.

Tenner T. J., Hirschmann M. M., Withers A. C. and Hervig R. L. (2009) Hydrogen partitioning between nominally anhydrous upper mantle minerals and melt between 3 and 5 GPa and applications to hydrous peridotite partial melting. *Chem. Geol.* **262**, 42–56.

Tian, Z., Chen, H., Fegley, Jr. B., Lodders, K., Barrat, J.A., Day, J.M.D., Wang (王昆), K., 2019. Potassium isotopic compositions of howardite-eucrite-diogenite meteorites. Geochim. Cosmochim. Acta, 266, 611–632.

Treiman A. H. (1997) The parent magmas of the cumulate eucrites: a mass balance approach. *Meteorit. Planet. Sci.* **32**, 217–230.

Treiman A. H., Lanzirotti A. and Xirouchakis D. (2004) Ancien water on asteroid 4 Vesta: evidence from a quartz veinlet in the Serra de Magé eucrite meteorite. *Earth Planet. Sci. Lett.* **219**, 189–199.

Treiman A., Boyce J. W., Greenwood J. P., Eiler J. M., Gross J., Guan Y., Ma C. and Stopler E. M. (2016) D-poor hydrogen in lunar mare basalts assimilated from lunar regolith. *Am. Mineral.* **101**(7), 1596–1603.

Usui T., Alexander C. M. O'D., Wang J., Simon J. I. and Jones J. H. (2012) Origin of water and mantle-crust interactions on Mars inferred from hydrogen isotopes and volatile element abundances of olivine-hosted melt inclusions of primitive shergottites. *Earth Planet. Sci. Lett.* **357–358**, 119–129.

Wade J. A., Plank T., Hauri E. H., Kelley K. A., Roggensack K. and Zimmer M. (2008) Prediction of magmatic water contents via measurement of H_2O in clinopyroxene phenocrysts. *Geology* **36**, 799–802.

Warren P. H. and Jerde E. A. (1987) Composition and origin of Nuevo Laredo Trend eucrites. *Geochim. Cosmochim. Acta* **51**, 713–725.

Warren J. M. and Hauri E. H. (2014) Pyroxenes as tracers of mantle water variations. *J. Geophys.: Res. Solid Earth* **119**, 1851–1881.

Weis F. A., Lazor P. and Skogby H. (2018) Hydrogen analysis in nominally anhydrous minerals by transmission Raman spectroscopy. *Phys. Chem. Miner.* **45**, 597–607.

Wiens R. C., Bochsler P., Burnett D. S. and Wimmer-Schweingruber R. F. (2004) Solar and solar wind isotopic compositions. *Earth Planet. Sci. Lett.* **226**, 549–565.

Wu J., Desch S. J., Schaefer L., Elkins-Tanton L. T., Pahlevan K. and Buseck P. R. (2018) Origin of earth's water: Chondritic inheritance plus nebular ingassing and storage of Hydrogen in the core. *J. Geophys. Res. Planets* **123**. https://doi.org/10.1029/2018JE005698.

Yamaguchi A., Taylor G. J. and Keil K. (1996) Global crustal metamorphism of the eucriteparent body. *Icarus* **124**, 97–112.

Yamaguchi A., Taylor G. J. and Keil K. (1997) Metamorphic history of the eucritic crustof 4 Vesta. *J. Geophys. Res.* **102**, 13381–13386.

Yamaguchi A., Barrat J. A., Greenwood R. C., Shirai N., Okamoto C., Setoyanagi T., Ebihara M., Franchi I. A. and Bohn M. (2009) Crustal partial melting on Vesta: Evidence from highly metamorphosed eucrites. *Geochim. Cosmochim. Acta* **73**, 7162–7182.

Yang X., Keppler H. and Li Y. (2016) Molecular hydrogen in mantle minerals. *Geochem. Perspect. Lett.* **2**, 160–168.

Associate editor: James M.D. Day